Linear-muffin-tin-orbital method for helical polymers: A detailed study of *trans*-polyacetylene

Michael Springborg
Fakultät für Chemie, Universität Konstanz, D-7750 Konstanz, Federal Republic of Germany

Jean-Louis Calais, Osvaldo Goscinski, and Leif A. Eriksson
Department of Quantum Chemistry, University of Uppsala, Box 518, S-75120 Uppsala, Sweden
(Received 28 March 1991)

Results of a detailed theoretical study of *trans*-polyacetylene are reported. In the first part, we present results on periodic chains which have been obtained with the first-principles, density-functional, full-potential linear-muffin-tin-orbital method for helical polymers. The lowest total energy is found for a structure with alternating carbon-carbon bond lengths in good agreement with experimental findings. Electronic band structures and densities of states are also presented. Moreover, photoelectron cross sections are determined and are used in calculating optical spectra, which are shown to agree well with experiments. A qualitative loss function is used in comparison with experimental electron-energy-loss spectra, and the results of Compton-scattering experiments are predicted. In the second part, we use the band structures, total energy, and Mulliken populations as functions of the structure in deriving a generalized, single-particle, Su-Schrieffer-Heeger model, which subsequently is used in studying solitons and polarons. It is found that solitons are stable distortions for the charged chains, and that the gap levels are placed about 0.1 eV from the midgap position. The lattice distortion, but not the electron or spin density, is more localized within the present model than with the Su-Schrieffer-Heeger model. Polarons, on the other hand, are found to be very shallow and most likely not stable.

I. INTRODUCTION

Polyacetylene was, to our knowledge, the first conjugated polymer for which a large doping-induced increase in electrical conductivity was reported.[1] Although similar effects have been found subsequently for a number of other conjugated polymers, polyacetylene has remained at the center of the research in these so-called conducting polymers (see, e.g., Ref. 2).

As is well known, the structure of the simplest form of polyacetylene, *trans*-polyacetylene (Fig. 1) contains zigzag chains of carbon atoms to which one hydrogen atom per carbon atom is attached. Since the σ bonds formed by carbon sp^2 hybrids and hydrogen $1s$ orbitals lie deep in energy, the frontier orbitals of a single chain are of π symmetry and formed by carbon p functions perpendicular to the plane of the nuclei. In a simple model one chain can thus be considered a quasi-one-dimensional system with one (π) electron per (CH) site, and it is as such expected to undergo a symmetry-lowering Peierls's distortion: a dimerization which opens up a gap at the Fermi level.

Ab initio Hartree-Fock calculations on structural properties of *trans*-polyacetylene have all been performed on isolated, single, finite, or infinite chains and have all found the lowest total energy for structures with alternating carbon-carbon bond lengths[3–14] in agreement with the above-mentioned picture. As demonstrated by Suhai[8,9] and by König and Stollhoff[14] inclusion of correlation effects in the *ab initio* Hartree-Fock calculations does not change this general conclusion.

On the other hand, first-principles density-functional calculations on *trans*-polyacetylene have been less conclusive. They have all been performed with a local approximation to the exchange and correlation effects but the examined systems range from isolated, finite, or infinite chains to three-dimensional, infinite, periodic crystals.[15–26] Most of those calculations have predicted a ground state with a nonvanishing carbon-carbon bond-length alternation, although the alternation often is underestimated compared with experimental findings. However, some of the most recent density-functional calculations have been interpreted as indicating that density-functional methods with a local approximation should find the lowest total energy to occur for a struc-

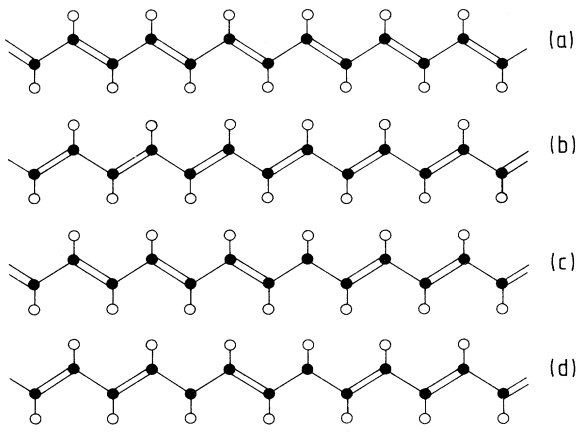

FIG. 1. Schematic representation of *trans*-polyacetylene. (a) and (b) show the two energetically degenerate ground-state forms, (c) a soliton, and (d) a polaron. Black (white) circles represent carbon (hydrogen) atoms.

ture with nonalternating C—C bond lengths.[22] Although the finding of Ashkenazi *et al.*[22] has been discussed,[14,25,27,28] no final conclusion has yet been obtained. Since a dimerization is clearly observed experimentally,[29,30] this is an unsatisfying situation and calls for further density-functional studies of the structure of *trans*-polyacetylene.

The density-functional full-potential LMTO (linear-muffin-tin-orbital) method for helical polymers[31] has been applied on a number of quasi-one-dimensional macromolecules during the last few years (see, e.g., Refs. 32 and 33). We have earlier[17] reported band structures of polyacetylene as obtained with this method plus results of a very limited geometry optimization. We will here report a much more detailed study of the total energy as a function of structure for a single, infinite periodic *trans*-polyacetylene chain. Compared with the earlier calculations[17] we have improved the quality of the present calculations by increasing lattice summations, number of basis functions, and number of terms included in internal summations. We therefore believe the present results to be close to the best possible with the present set of computer codes.

In order to be able to evaluate the quality of the calculations we have also calculated various quantities that are directly accessible experimentally. These include photoelectron spectra, joint densities of states, and reciprocal-form factors, as can be determined in optical experiments, electron-energy-loss experiments, and Compton scattering, respectively. The calculations of these quantities represent extensions of our computational scheme and we therefore include a more precise description of how they are calculated.

Su, Schrieffer, and Heeger (SSH) have presented a model[34,35] that qualitatively accounts for the doping-induced increase in electrical conductivity and a number of other experimental findings. They noticed that *trans*-polyacetylene has two energetically degenerate structures [the so-called *A* and *B* phases, Figs. 1(a) and 1(b)] only differing in the C—C bond-order alternation, such that domain-walls in single chains separating parts of the chain with different phases [the so-called solitons[34] or misfits;[36] Fig. 1(c)] will be highly mobile. With a simple model including a tight-binding description of the π electrons ($\hat{H}_\pi$) and a harmonic approximation for the remainder ($\hat{H}_\sigma$) of the total energy they could demonstrate that the solitons were (meta)stable for the charged and neutral chains.

It is, however, not clear whether a single-particle model is appropriate for the conducting polymers, and it has thus been discussed whether the differences between the details of the experimental findings and the details of the predictions of the SSH model are due to single- or many-body effects (see, e.g., Refs. 37 and 38).

The density-functional method has the advantage that the results can easily be mapped on a single-particle model which subsequently can be compared with the SSH model. Such a procedure has recently been undertaken for the related system of a linear carbon chain.[39] It was there found that $\hat{H}_\sigma$ contained anharmonic contributions that led to polarons and not solitons being the stable quasiparticles for charged chains. Another purpose of the present paper is thus to derive a modified single-particle SSH model for *trans*-polyacetylene and, subsequently, to study the consequences of the modifications compared to the original SSH model.

The paper is organized as follows. In order for the paper to be self-containing we give some details of the computational method in Sec. II, as otherwise in detail described in Ref. 31. In Sec. III we discuss two different expressions for the total energy and present our optimized structure for *trans*-polyacetylene. Section IV gives the band structures, and in Sec. V Mulliken populations are presented. Densities of states and photoelectron spectra are presented in Sec. VI, and electron-energy-loss spectra in Sec. VII. The electron densities in momentum space are calculated in Sec. VIII, and in Sec. IX we report the reciprocal form factors. In Sec. X we derive our modified SSH model for *trans*-polyacetylene, and Sec. XI contains the results from the model calculations on chains containing solitons and polarons. We finally conclude in Sec. XII.

II. THE LMTO METHOD FOR HELICAL POLYMERS

A. The LMTO's

Within the Born-Oppenheimer approximation and the density-functional formalism[40] the time-independent electronic ground-state energy of any (finite or infinite) molecule can be obtained by solving the single-particle Kohn-Sham equations[41] (in Ry atomic units)

$$[-\nabla^2+V(\mathbf{r})]\psi_i(\mathbf{r})=\varepsilon_i\psi_i(\mathbf{r}) \ . \tag{1}$$

The electronic density is then given as the sum over the occupied orbitals

$$\rho(\mathbf{r})=\sum_{i=1}^{\text{occ}} |\psi_i(\mathbf{r})|^2 \ , \tag{2}$$

and the ground-state energy can be derived from the functions ψ_i and the energies ε_i as described in Sec. III.

As is well known, the potential $V(\mathbf{r})$ in Eq. (1) is the sum of the Coulomb potentials of the nuclei (V_N) and of the electron density (V_C), plus the remaining exchange-correlation potential (V_{xc}) which in the local approximation is approximated by a function of the density (2). Thus,

$$V(\mathbf{r})=V_N(\mathbf{r})+V_C(\mathbf{r})+V_{\text{xc}}(\mathbf{r}) \ , \tag{3}$$

with

$$\nabla^2 V_C(\mathbf{r})=-8\pi\rho(\mathbf{r}) \tag{4}$$

and

$$V_{\text{xc}}(\mathbf{r})=V_{\text{xc}}[\rho(\mathbf{r})] \ , \tag{5}$$

such that in solving Eqs. (1)–(5), self-consistency is required, i.e., the potential entering Eq. (1) is to be identical to that obtained from Eqs. (2)–(5).

Although no formal justification exists we will throughout the paper assume that the single-particle eigenvalues ε_i of Eq. (1) are good approximations to the

electronic excitation energies, as experience has shown most often to be the case (see, e.g., Ref. 42).

We expand the eigenfunctions $\psi_i(\mathbf{r})$ of Eq. (1) in a basis of LMTO's which is defined as follows. Nonoverlapping (muffin-tin) spheres are defined such that each nucleus occupies a center. Replacing $V(\mathbf{r})$ of Eq. (1) with its spherically symmetric component and choosing $\varepsilon=\varepsilon_{\nu RL}$ "reasonable" (i.e., in the energy interval for which that particular function is of interest), the resulting Kohn-Sham equations

$$[-\nabla^2+V_{\mathbf{R}}(r_{\mathbf{R}})]\phi_{\mathbf{R}L}(\mathbf{r}_{\mathbf{R}})=\varepsilon_{\nu RL}\phi_{\mathbf{R}L}(\mathbf{r}_{\mathbf{R}}) \tag{6}$$

become one-dimensional and can be solved numerically inside each sphere. Here, $\mathbf{R}$ is a site index, $L\equiv(l,m)$, $\mathbf{r}_{\mathbf{R}}=\mathbf{r}-\mathbf{R}$, and $V_{\mathbf{R}}(r_{\mathbf{R}})$ is the spherically symmetric part of the potential inside the sphere at $\mathbf{R}$.

$\phi_{\mathbf{R}L}$ depends parametrically on $\varepsilon_{\nu RL}$ so we can define the derivative

$$\dot{\phi}_{\mathbf{R}L}(\mathbf{r}_{\mathbf{R}})=\frac{\partial\phi_{\mathbf{R}L}(\mathbf{r}_{\mathbf{R}})}{\partial\varepsilon_{\nu RL}} \tag{7}$$

and from ϕ and $\dot{\phi}$ we form the linear combinations

$$\begin{aligned}\phi_{\mathbf{R}L}(\mathbf{r}_{\mathbf{R}})+\omega^K_{\mathbf{R}L}(\kappa)\dot{\phi}_{\mathbf{R}L}(\mathbf{r}_{\mathbf{R}})&\\ =[\phi_{\mathbf{R}L}(r_{\mathbf{R}})+\omega^K_{\mathbf{R}L}(\kappa)\dot{\phi}_{\mathbf{R}L}(r_{\mathbf{R}})]Y_L(\hat{\mathbf{r}}_{\mathbf{R}})\ ,&\end{aligned} \tag{8}$$

such that they match continuously and differentiably with

$$\begin{aligned}c^K_{\mathbf{R}L}(\kappa)K_{\mathbf{R}L}(\kappa;\mathbf{r}_{\mathbf{R}})&\equiv c^K_{\mathbf{R}L}(\kappa)K_{\mathbf{R}L}(\kappa;r_{\mathbf{R}})Y_L(\hat{\mathbf{r}}_{\mathbf{R}})\\ &\equiv c^K_{\mathbf{R}L}(\kappa)\frac{i\kappa^{l+1}}{(2l-1)!!}h_l^{(1)}(\kappa r_{\mathbf{R}})Y_L(\hat{\mathbf{r}}_{\mathbf{R}})\ .\end{aligned} \tag{9}$$

Here c is a constant, $h_l^{(1)}$ is a spherical Hankel function of first kind, and κ is purely imaginary. $r_{\mathbf{R}}$ and $\hat{\mathbf{r}}_{\mathbf{R}}$ are the radial and angular parts of $\mathbf{r}_{\mathbf{R}}$, respectively.

Inside any other sphere, say at $\mathbf{R}'$, we make use of the expansion

$$K_{\mathbf{R}L}(\kappa;\mathbf{r}_{\mathbf{R}})=\sum_{L'}S_{LL'}(\kappa;\mathbf{R}-\mathbf{R}')J_{\mathbf{R}'L'}(\kappa;\mathbf{r}_{\mathbf{R}'})\ , \tag{10}$$

with

$$\begin{aligned}J_{\mathbf{R}'L'}(\kappa;\mathbf{r}_{\mathbf{R}'})&\equiv J_{\mathbf{R}'L'}(\kappa;r_{\mathbf{R}'})Y_{L'}(\hat{\mathbf{r}}_{\mathbf{R}'})\\ &\equiv\tfrac{1}{2}(2l'-1)!!\kappa^{-l'}j_{l'}(\kappa r_{\mathbf{R}'})Y_{L'}(\hat{\mathbf{r}}_{\mathbf{R}'})\end{aligned} \tag{11}$$

and $j_{l'}$ being a spherical Bessel function. We then replace in Eq. (10), term by term, $J_{\mathbf{R}'L'}(\kappa;\mathbf{r}_{\mathbf{R}'})$ by

$$[c^J_{\mathbf{R}'L'}(\kappa)]^{-1}[\phi_{\mathbf{R}'L'}(\mathbf{r}_{\mathbf{R}'})+\omega^J_{\mathbf{R}'L'}(\kappa)\dot{\phi}_{\mathbf{R}'L'}(\mathbf{r}_{\mathbf{R}'})]\ , \tag{12}$$

such that (11) and (12) are continuous and differentiable on the boundary of the sphere at $\mathbf{R}'$.

Our experience has shown that good accuracy is achieved with a basis set consisting of two subsets, each having one common κ for all $\mathbf{R}$ and L, and with s, p, and d functions on all sites.

$$\psi_i(\mathbf{r})=\sum_{\kappa\mathbf{R}L}\eta_{i\kappa\mathbf{R}L}\chi_{\mathbf{R}L\kappa}(\mathbf{r})=\begin{cases}\sum_{\mathbf{R}L}[a_{i\mathbf{R}L}\phi_{\mathbf{R}L}(\mathbf{r}_{\mathbf{R}})+b_{i\mathbf{R}L}\dot{\phi}(\mathbf{r}_{\mathbf{R}})] & \text{inside the muffin-tin spheres}\\ \sum_{\kappa\mathbf{R}L}d_{i\kappa\mathbf{R}L}K_{\mathbf{R}L}(\kappa;\mathbf{r}_{\mathbf{R}}) & \text{in the interstitial region}\ ,\end{cases} \tag{13}$$

with $\chi_{\mathbf{R}L\kappa}$ being a LMTO centered at site $\mathbf{R}$. We will not discuss further how one explicitly determines the coefficients η, a, b, and d in Eq. (13), and refer the reader to Ref. 31. We will here only mention a few things. First of all, although the LMTO's are eigenfunctions to a muffin-tin potential, this does not imply that the potential is assumed to be of muffin-tin form. The full potential is included in the calculations but the muffin-tin potential offers a way of defining a limited basis set consisting of functions that are good approximations to the exact solutions to Eq. (1). Moreover, in order to solve the Poisson equation (4) in the interstitial region we make there a least-squares fit of the electron density (see Ref. 31), i.e.,

$$\begin{aligned}\rho(\mathbf{r})&=\sum_{i=1}^{\text{occ}}\sum_{\kappa_1\kappa_2}\sum_{\mathbf{R}_1\mathbf{R}_2}\sum_{L_1L_2}d^*_{i\kappa_1\mathbf{R}_1L_1}d_{i\kappa_2\mathbf{R}_2L_2}K^*_{\mathbf{R}_1L_1}(\kappa_1;\mathbf{r}_{\mathbf{R}_1})\\ &\quad\times K_{\mathbf{R}_2L_2}(\kappa_2;\mathbf{r}_{\mathbf{R}_2})\\ &\simeq\tilde{\rho}(\mathbf{r})=\sum_{\lambda}\sum_{\mathbf{R}}\sum_{L}\rho_{\lambda\mathbf{R}L}K_{\mathbf{R}L}(\lambda;\mathbf{r}_{\mathbf{R}})\ .\end{aligned} \tag{14}$$

The least-squares fit gives the coefficients $\rho_{\lambda\mathbf{R}L}$. Also the exchange-correlation potential is approximated in the interstitial region

$$V_{\text{xc}}(\mathbf{r})\simeq\tilde{V}_{\text{xc}}(\mathbf{r})\ . \tag{15}$$

In Sec. III we will discuss some of the implications on the total energy due to the fit.

B. Helical polymers

First of all, the discussion in this section is not restricted to the present LMTO method but can be applied for any method which makes use of a basis set of atom-centered functions. We will classify any large molecule which has screw-axis symmetry and for which the intermolecular interactions are negligible compared to the intramolecular interactions as a helical polymer. The primitive screw-axis symmetry operation is a combined translation (of h) and rotation (of v), and in a global

right-handed coordinate system with the z axis parallel to the screw axis the position of the ith atom in the nth unit cell is

$$x = r_i \cos u_{ni} ,$$
$$y = r_i \sin u_{ni} , \tag{16}$$
$$z = (h/v)u_{ni} + z_i ,$$

with

$$u_{ni} = nv + \phi_i . \tag{17}$$

r_i, ϕ_i, and z_i are unique for the ith atom. Any helical polymer can thus be described with $3N+2$ parameters of which, however, one of the ϕ_i and one of the z_i can be fixed arbitrarily leaving $3N$ internal degrees of freedom.

Bloch waves that are adapted to the screw-axis symmetry can be constructed from atom-centered basis functions that are defined in local, atom-centered, right-handed coordinate systems with the z axis parallel to and the x axis pointing away from the screw axis. Denoting such an atom-centered function $\chi_{\mathbf{R}nL\kappa}$ with $\mathbf{R}$, n, L, and κ being site index, unit-cell index, (l,m), and any other parameters specifying the function, respectively, the Bloch waves become

$$\chi^k_{\mathbf{R}L\kappa} = (2M+1)^{-1/2} \sum_{n=-M}^{M} \chi_{\mathbf{R}nL\kappa} e^{in\pi k} . \tag{18}$$

Here, Born–von-Kármán periodic boundary conditions have been applied and M is a large but finite integer. Moreover, k is a reduced wave number which in the special case of pure translational symmetry ($v = 2\pi$; unit-cell length h) reduces to

$$k = k'h/\pi , \tag{19}$$

where k' is the standard wave number. The first Brillouin zone is defined by

$$k \in [-1,1] . \tag{20}$$

With the basis set of Eq. (18) we can finally write the general eigenvector as

$$\psi^k_j = \sum_{\mathbf{R}L\kappa} a^k_{j,\mathbf{R}L\kappa} \chi^k_{\mathbf{R}L\kappa}$$
$$= (2M+1)^{-1/2} \sum_{\mathbf{R}L\kappa} \sum_{n=-M}^{M} a^k_{j,\mathbf{R}L\kappa} \chi_{\mathbf{R}nL\kappa} e^{in\pi k} , \tag{21}$$

where the coefficients $a^k_{j,\mathbf{R}L\kappa}$ are to be determined in the self-consistent calculations.

III. TOTAL ENERGY AND STRUCTURE

A. Two expressions for the total energy

For a compound for which the densities of the core electrons are assumed identical to those of the isolated atoms (i.e., frozen) we will only consider that part of the total energy which changes upon forming the compound from the isolated atoms. This "valence energy" is

$$E_{\mathrm{val}} = \sum_{i=1}^{\mathrm{occ}} \langle \psi_i | (-\nabla^2) | \psi_i \rangle + \int \rho_v(\mathbf{r}) [\tfrac{1}{2} V_v(\mathbf{r}) + V_{Nc}(\mathbf{r})] d\mathbf{r}$$
$$+ E_{\mathrm{xc}}[\rho_c(\mathbf{r}) + \rho_v(\mathbf{r})] - E_{\mathrm{xc}}[\rho_c(\mathbf{r})] + \sum_{i \neq j} \frac{Z_{ci} Z_{cj}}{|\mathbf{R}_i - \mathbf{R}_j|} . \tag{22}$$

Here ρ_v and ρ_c are the valence and core electron densities, respectively, V_v is the Coulomb potential of the valence electrons, V_{Nc} is that of the core electrons and the nuclei, E_{xc} is the exchange-correlation energy functional, Z_{ci} is the effective nuclear charge (i.e., sum of nuclear and core charges), and $\mathbf{R}_i$ is the position of the ith nucleus.

With the present method we cannot directly evaluate Eq. (22). First of all, in the interstitial region (IR) both V_v and E_{xc} are approximated [see, e.g., Eqs. (14) and (15)]. In evaluating the interstitial part of the integral in Eq. (22) we write in the interstitial region

$$\rho_v(\mathbf{r}) = \tilde{\rho}_v(\mathbf{r}) + \Delta\rho_v(\mathbf{r}) . \tag{23}$$

Then first-order terms in the error $\Delta\rho_v$ can be eliminated through

$$\int_{\mathrm{IR}} \rho_v(\mathbf{r}) V_v(\mathbf{r}) d\mathbf{r} \simeq 2 \int_{\mathrm{IR}} \rho_v(\mathbf{r}) \tilde{V}_v(\mathbf{r}) d\mathbf{r} - \int_{\mathrm{IR}} \tilde{\rho}_v(\mathbf{r}) \tilde{V}_v(\mathbf{r}) d\mathbf{r} , \tag{24}$$

as demonstrated by, e.g., Dunlap, Connolly, and Sabin.[43] Here, "IR" is used for "interstitial region," and $\tilde{V}_v$ is the Coulomb potential due to $\tilde{\rho}_v$.

Similarly, since

$$E_{\mathrm{xc}}[\rho(\mathbf{r})] = \int \varepsilon_{\mathrm{xc}}[\rho(\mathbf{r})] \rho(\mathbf{r}) d\mathbf{r} , \tag{25}$$

and $\varepsilon_{\mathrm{xc}}$ is dominated by a term proportional to $\rho^{4/3}$, a good approximation to the exchange-correlation energy contribution from the interstitial region is (assuming the core electrons to be confined to the muffin-tin spheres)

$$\int_{\mathrm{IR}} \varepsilon_{\mathrm{xc}}[\rho_v(\mathbf{r}) + \rho_c(\mathbf{r})][\rho_v(\mathbf{r}) + \rho_c(\mathbf{r})] d\mathbf{r}$$
$$= \int_{\mathrm{IR}} \varepsilon_{\mathrm{xc}}[\rho_v(\mathbf{r})] \rho_v(\mathbf{r}) d\mathbf{r}$$
$$\simeq \tfrac{4}{3} \int_{\mathrm{IR}} \tilde{\varepsilon}_{\mathrm{xc}}(\mathbf{r}) \rho_v(\mathbf{r}) d\mathbf{r} - \tfrac{1}{3} \int_{\mathrm{IR}} \tilde{\varepsilon}_{\mathrm{xc}}(\mathbf{r}) \tilde{\rho}_v(\mathbf{r}) d\mathbf{r} . \tag{26}$$

Moreover, since a calculation requires iterating until self-consistency is reached, it is important to notice that the evaluation of E_{val} in the nth iteration requires calculation of ρ_v, E_x, and V_v from the eigenfunctions ψ_i of that iteration. We will indicate this by superscripts (n) on the quantities involved.

We now notice that the function $\psi^{(n)}_i$ is a solution to the Kohn-Sham equations (1) for the potential

$$V^{(n-1)}(\mathbf{r})=V_{Nc}(\mathbf{r})+V_v^{(n-1)}(\mathbf{r})+V_{\mathrm{xc}}[\rho_v^{(n-1)}(\mathbf{r})+\rho_c(\mathbf{r})] \tag{27}$$

and corresponding to the eigenvalue $\varepsilon_i^{(n)}$. Therefore,

$$\langle\psi_i^{(n)}|(-\nabla^2)|\psi_i^{(n)}\rangle=\langle\psi_i^{(n)}|[\varepsilon_i^{(n)}-V^{(n-1)}(\mathbf{r})]|\psi_i^{(n)}\rangle\ . \tag{28}$$

In evaluating the first term on the right-hand side of Eq. (22) one may thus use either the left-hand or the right-hand side of Eq. (28). This leaves us with two different expressions for $E_{\mathrm{val}}^{(n)}$, which both can be written as ("MTS" denoting muffin-tin spheres)

$$E_{\mathrm{val}}^{(n)}=E_0^{(n)}+\int_{\mathrm{MTS}}\rho_v^{(n)}(\mathbf{r})e_1^{(n)}(\mathbf{r})d\mathbf{r}+\int_{\mathrm{MTS}}\rho_c(\mathbf{r})\varepsilon_{\mathrm{xc}}[\rho_v^{(n)}(\mathbf{r})+\rho_c(\mathbf{r})]d\mathbf{r}$$
$$+\int_{\mathrm{IR}}\rho_v^{(n)}(\mathbf{r})e_2^{(n)}(\mathbf{r})d\mathbf{r}+\int_{\mathrm{IR}}\tilde{\rho}_v^{(n)}(\mathbf{r})[-\tfrac{1}{2}\tilde{V}_v^{(n)}(\mathbf{r})-\tfrac{1}{3}\tilde{\varepsilon}_{\mathrm{xc}}^{(n)}(\mathbf{r})]d\mathbf{r}-\int_{\mathrm{MTS}}\rho_c(\mathbf{r})\varepsilon_{\mathrm{xc}}[\rho_c(\mathbf{r})]d\mathbf{r}+\sum_{i\neq j}\frac{Z_{ci}Z_{cj}}{|\mathbf{R}_i-\mathbf{R}_j|}\ , \tag{29}$$

with either

$$E_0^{(n)}=\sum_{i=1}^{\mathrm{occ}}\langle\psi_i^{(n)}|(-\nabla^2)|\psi_i^{(n)}\rangle\ ,$$
$$e_1^{(n)}(\mathbf{r})=\tfrac{1}{2}V_v^{(n)}(\mathbf{r})+V_{Nc}(\mathbf{r})+\varepsilon_{\mathrm{xc}}[\rho_v^{(n)}(\mathbf{r})+\rho_c(\mathbf{r})]\ , \tag{30}$$
$$e_2^{(n)}(\mathbf{r})=\tilde{V}_v^{(n)}(\mathbf{r})+V_{Nc}(\mathbf{r})+\tfrac{4}{3}\varepsilon_{\mathrm{xc}}^{(n)}(\mathbf{r})\ ,$$

or

$$E_0^{(n)}=\sum_{i=1}^{\mathrm{occ}}\varepsilon_i^{(n)}\ ,$$
$$e_1^{(n)}(\mathbf{r})=\tfrac{1}{2}V_v^{(n)}(\mathbf{r})-V_v^{(n-1)}(\mathbf{r})+\varepsilon_{\mathrm{xc}}[\rho_v^{(n)}(\mathbf{r})+\rho_c(\mathbf{r})]$$
$$-V_{\mathrm{xc}}[\rho_v^{(n-1)}(\mathbf{r})+\rho_c(\mathbf{r})]\ , \tag{31}$$
$$e_2^{(n)}(\mathbf{r})=\tilde{V}_v^{(n)}(\mathbf{r})-\tilde{V}_v^{(n-1)}(\mathbf{r})+\tfrac{4}{3}\tilde{\varepsilon}_{\mathrm{xc}}^{(n)}(\mathbf{r})-\tilde{V}_{\mathrm{xc}}^{(n-1)}(\mathbf{r})\ .$$

Equations (30) and (31) each has its advantages over the other. Thus, the eigenvalue sum in Eq. (31) makes the analogy to tight-binding approaches obvious, whereas the simple form of the integrands as products of densities and potentials (in contrast to differences of potentials) makes detailed analysis possible with Eq. (30); for instance, the sphere integrals can be separated into spherically symmetric components and remainders, and the effects of the latter—excluded in some approaches—can be studied.

B. Test systems

The two total-energy expressions should in principle be identical but in practice are not. Numerical problems related to the diagonalization of the Hamiltonian and to the fitting of the interstitial densities, due to almost linear dependences and accordingly almost singular matrices, are one source of errors. Also the fact that our calculated solutions to the Kohn-Sham equations are not the *exact* ones due to the expansion in a finite basis set lead to discrepancies. Furthermore, for infinite, periodic systems the truncation of the lattice sums after a finite number of terms influences the two expressions differently. This is, finally, also the case for the infinite summations related to the interstitial matrix elements (see Ref. 31). Comparison of the two expressions thus gives information about the accuracy of the calculation.

In order to obtain a more detailed understanding of the differences in the two total-energy expressions (ΔE), we performed more series of test calculations on some simpler systems at various levels of accuracy. We first considered five cases of a single diatomic molecule. For three of those the molecules were homonuclear, H_2, N_2, and Br_2, and for two they were heteronuclear, CO and LiF. We could thereby to some extent isolate the effects of Coulomb forces due to a charge transfer.

The electron density in H_2 is very smooth such that angular expansions thereof are rapidly convergent. Therefore, ΔE was found to be small and almost independent on sphere radii and series truncations. On the other hand, the bond in N_2 is highly anisotropic such that the electron density is rapidly varying. It turned out that it was important to have a proper description of the electron density inside the spheres in order to keep ΔE small. Especially the first integral in Eq. (29) (involving e_2) was to be evaluated accurately. It was necessary to include at least d terms in the expansions of the electron density and the Coulomb potential inside the sphere.

The CO molecule is very similar to the N_2 molecule having the same number of electrons. It is accordingly not surprising that the results found for N_2 were recovered for CO. However, the chemical bond of the CO molecule has an ionic component absent for the N_2 molecule. The potential due to this charge transfer is smooth and therefore well accounted for by angular components of low l of the Coulomb potential. ΔE is therefore in general smaller for CO than for N_2 for otherwise equivalent calculations.

The electron density in the LiF molecule is closer to being spherically symmetric around the nuclei than those of the N_2 and CO molecules. ΔE was therefore for the LiF molecule generally small and hardly sensitive to cutoffs in angular expansions.

The Br_2 molecule is larger and there are more electrons inside the spheres. For this it turned out that in calculating the exchange-correlation energy and potential inside the spheres it was necessary to allow these to be nonspherically symmetric and to use the full electron density

in their evaluation rather than just the spherical average. This is a generalization of the original procedure described in Ref. 31.

We then tested lattice summations in direct and reciprocal space by studying Se and HF chains. The main extension of the conclusions above for the finite molecules was that in order to keep ΔE small it was important to include many unit cells in evaluating potentials of the r^{-1} form as generated by the electron density. Although the total long-range r^{-1} potential vanishes due to charge neutrality, it is important to evaluate each term separately with care. Since the second total-energy expression [Eq. (30)] involves differences of potentials, we believe this to be less sensitive to inaccuracies to lattice summations due to lucky cancellations of errors.

Finally, it turned out in all the test calculations that once a well-converged set of calculations was determined, ΔE was almost independent of the structure of the finite or infinite system. Moreover, calculations keeping only the spherically symmetric terms inside the muffin-tin spheres usually led to a small ΔE, but the structural properties (e.g., bond lengths) were often poorly reproduced by such calculations.

C. *Trans*-polyacetylene

For *trans*-polyacetylene we considered chains with one C_2H_2 unit per unit cell. We assumed the H atoms to lie along the negative C—C—C bond angle bisectors with a C—H bond length of 2.10 a.u. Exploratory calculations on an undimerized chain with one CH unit per unit cell gave that the optimized C—H bond length would lie between 2.05 and 2.10 a.u.

Assuming the polymer to be planar we subsequently optimized the two C—C bond lengths (d_1 and d_2) and the C—C—C bond angle (β). The lowest total energy (independent of which expression was chosen) was found for $d_1=2.58$ a.u.$=1.36$ Å, $d_2=2.76$ a.u.$=1.46$ Å, and $\beta=128°$. These bond lengths agree well with experimental values; $d_1=1.36$ Å and $d_2=1.44$ Å.[30] Moreover, *ab initio* Hartree-Fock calculations have all predicted a nonvanishing bond-length alternation: $d_1=1.32-1.37$ Å and $d_2=1.43-1.48$ Å (Refs. 3, 4, 6, 7, and 9–14), as well as $\beta=124°-125°$.[3,6,7,9,10,13]

Other density-functional calculations on a single chain have also predicted $d_1\neq d_2$. Thus, Mintmire and White[15,16] found in their earliest work $(d_1,d_2)=(1.38$ Å, 1.43 Å). They reported later,[20] however, that the bond-length alternation decreases as a function of the number of k points included in the calculations giving $(d_1,d_2)=(1.40$ Å, 1.43 Å) for their most complete set of k points. Earlier calculations[17,18] with the present method resulted in (1.36 Å, 1.44 Å), which, however, only may be considered preliminary due to the very limited geometry variations. More recent, detailed studies of finite C_nH_{n+2} molecules[26] gave $(d_1,d_2)=(1.36$ Å, 1.42 Å) for $n=20$. This value of n must be considered sufficiently large such that the bond-length alternation has converged to its value for $n\rightarrow\infty$.

On the other hand, the density-functional calculations on crystalline *trans*-polyacetylene have given either a very small[19,23–25] or a vanishing[22] bond-length alternation. Although in the last case (Ref. 22) it was argued that these results were also found for single chains, the single-chain results were actually found for calculations on a hypothetic three-dimensional structure with a large interchain distance, and it can thus not be excluded that these calculations were less well converged than the others (e.g., it is difficult to expand electronic orbitals which are localized in one or more directions in a plane-wave basis set). Therefore, it is possible that the finding of a small dimerization amplitude in some density-functional studies is a consequence of interchain interactions, since these may have significant impacts on the structure.[44] This, in turn, may be related to the tendency of local-density methods in overestimating the strength of any chemical bond.[42]

As this discussion may indicate, the origin of the force driving the observed bond-length alternation in *trans*-polyacetylene cannot be considered fully understood. Our results suggest a simple Peierls's mechanism, but we cannot definitively exclude other possibilities.

IV. THE BAND STRUCTURES OF *TRANS*-POLYACETYLENE

In Fig. 2 we show the band structures for our optimized structure. We have earlier[17] given a detailed account of a number of sets of theoretical band structures including a set obtained with the same method as used here. However, as mentioned above the present calculations are better converged and, moreover, the geometry has been optimized. We will here only compare with those of Ref. 17 as well as with some more recent sets of band structures. A comparison with experimental information on the band structures will be presented in Secs. VI and VII.

Compared with our bands in Ref. 17 the overlap be-

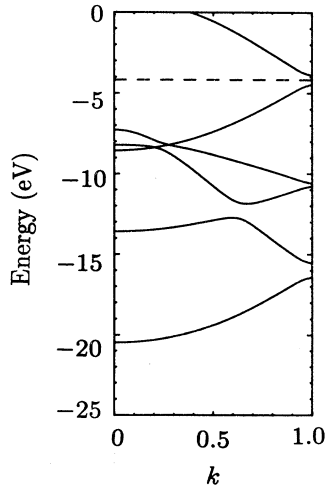

FIG. 2. The calculated band structures of *trans*-polyacetylene. Only the valence bands and the lowest conduction band are shown. The dashed line represents the Fermi level, and $k=0$ and 1 are the zone center and zone edge, respectively.

tween σ and π valence bands in Fig. 2 is smaller and in better agreement with the findings of other theoretical methods. Moreover, the total valence-band width is slightly less than 1 eV smaller in Fig. 2 than in Ref. 17, which may be due to differences in the C—C—C bond angle. Finally, the ionization potential in Fig. 2 is about 1 eV smaller than that of Ref. 17.

Only a few other sets of theoretical band structures or density of states have been presented since Ref. 17 was published. Of the density-functional calculations our valence-band width agrees well with that found on a single chain by one of us,[45] on a finite cluster by Ye *et al.*,[26] and on a crystal by Vogl and Campbell,[25] whereas that found by von Boehm, Kuivalainen, and Calais[46] on a single chain is slightly larger. On the other hand, the methods based on the Hartree-Fock approximation overestimate this width significantly, as can be observed in Refs. 12 and 47.

The band gap in Fig. 2 (0.6 eV) is substantially underestimated compared with the experimental value (about 1.6 eV; Ref. 48), as is a well-known artifact of density-functional calculations incorporating a local-density approximation. In total we find the valence-band structures of Fig. 2 trustworthy, as we shall further see in Secs. VI and VII.

V. MULLIKEN POPULATIONS

A. Formulas

The normalization of the Bloch wave of Eq. (21) gives

$$
\begin{aligned}
1 &= (2M+1)^{-1} \sum_{\mathbf{R}_1 L_1 \kappa_1} \sum_{\mathbf{R}_2 L_2 \kappa_2} \sum_{n_1, n_2 = -M}^{M} (a^k_{j,\mathbf{R}_1 L_1 \kappa_1})^* (a^k_{j,\mathbf{R}_2 L_2 \kappa_2}) \langle \chi_{\mathbf{R}_1 n_1 L_1 \kappa_1} | \chi_{\mathbf{R}_2 n_2 L_2 \kappa_2} \rangle e^{i\pi k (n_2 - n_1)} \\
&= \sum_{\mathbf{R}_1 L_1 \kappa_1} \sum_{\mathbf{R}_2 L_2 \kappa_2} \sum_{n=-M}^{M} (a^k_{j,\mathbf{R}_1 L_1 \kappa_1})^* (a^k_{j,\mathbf{R}_2 L_2 \kappa_2}) \langle \chi_{\mathbf{R}_1 0 L_1 \kappa_1} | \chi_{\mathbf{R}_2 n L_2 \kappa_2} \rangle e^{i\pi k n} \\
&= \sum_{\mathbf{R}} \sum_{L_1 \kappa_1} \sum_{L_2 \kappa_2} \sum_{n=-M}^{M} (a^k_{j,\mathbf{R} L_1 \kappa_1})^* (a^k_{j,\mathbf{R} L_2 \kappa_2}) \langle \chi_{\mathbf{R} 0 L_1 \kappa_1} | \chi_{\mathbf{R} n L_2 \kappa_2} \rangle e^{i\pi k n} \\
&\quad + \sum_{\mathbf{R}_1 \neq \mathbf{R}_2} \sum_{L_1 \kappa_1} \sum_{L_2 \kappa_2} \sum_{n=-M}^{M} (a^k_{j,\mathbf{R}_1 L_1 \kappa_1})^* (a^k_{j,\mathbf{R}_2 L_2 \kappa_2}) \langle \chi_{\mathbf{R}_1 0 L_1 \kappa_1} | \chi_{\mathbf{R}_2 n L_2 \kappa_2} \rangle e^{i\pi k n} \\
&\equiv \sum_{\mathbf{R}} n^k_{j,\mathbf{R}} + \sum_{\mathbf{R}_1 \neq \mathbf{R}_2} n^k_{j,\mathbf{R}_1 \mathbf{R}_2} \, .
\end{aligned} \tag{32}
$$

This is just the standard procedure originally due to Mulliken[49] of dividing the electron density from the function of Eq. (21) into atomic net populations ($n^k_{j,\mathbf{R}}$) and overlap populations ($n^k_{j,\mathbf{R}_1\mathbf{R}_2}$). We notice, however, that in this simplest approach the atomic net populations contain contributions from overlap populations between equivalent atoms from different unit cells. Similarly, the overlap populations are those between orbitals centered on one type of atoms and orbitals centered on *all* the equivalent atoms of the other type. Without further decomposing Eq. (32) it is not possible to distinguish between intra-unit-cell components and inter-unit-cell components. A more detailed decomposition which avoids this ambiguity has been introduced by Hughbanks and Hoffmann.[50]

Finally, gross populations $N^k_{j,\mathbf{R}}$ are defined as usual from Eq. (32) by writing

$$
1 = \sum_{\mathbf{R}} \left[n^k_{j,\mathbf{R}} + \tfrac{1}{2} \sum_{\mathbf{R}' \neq \mathbf{R}} n^k_{j,\mathbf{R}\mathbf{R}'} \right] \equiv \sum_{\mathbf{R}} N^k_{j,\mathbf{R}} \tag{33}
$$

and by summing the different populations over the occupied orbitals (i.e., over j and k) total (net, overlap, or gross) populations are obtained.

B. *Trans*-polyacetylene

With the help of the Mulliken populations it is easy to interpret the band structures of Fig. 2. Among the σ valence bands we recognize two avoided crossings (one between the σ_2 and σ_3 bands and one between the σ_3 and σ_4 bands). For a hypothetic case with the bands of Fig. 2 unfolded about $k=1$ (corresponding to an undimerized chain) and with no avoided crossings we would thus have one broad valence band between roughly -20 and -7 eV and one narrower between -14 and -8 eV. Since only the latter has significant hydrogen populations, this is the one generated by the C-H σ bonds and the other band is then due to the C-C σ bonds.

The Mulliken populations give one more important piece of information. The π bands have only very small components on the hydrogen atoms. This will become of importance in Sec. X.

VI. DENSITY OF STATES AND PHOTOELECTRON SPECTRA

A. Theory

The discussion of the present section follows closely that of Mintmire and White[16,51] with the modification,

however, that we use LMTO's as basis functions, whereas they use Gaussians.

The differential photoelectron cross section for the jth electronic orbital is[52]

$$\frac{d\sigma_j(\mathbf{k}_f)}{d\Omega}=\frac{2L^3k_f}{3\pi c\omega}|\mathbf{P}_j|^2 , \tag{34}$$

with

$$\mathbf{P}_j=\int \psi^*_{\mathbf{k}_f}(\mathbf{r})\nabla\psi_j(\mathbf{r})d\mathbf{r} . \tag{35}$$

Here ω is the energy of the incoming photon, $\mathbf{k}_f$ and $\psi_{\mathbf{k}_f}$ are the wave number and wave function of the scattered electron, respectively, L^3 is the volume of the sample, and ψ_j is the wave function of the electron before being scattered. Relaxation effects are neglected, and we will assume the wave function of the scattered (out going) electron to be a plane wave

$$\psi_{\mathbf{k}_f}(\mathbf{r})=L^{-3/2}e^{i\mathbf{k}_f\cdot\mathbf{r}} . \tag{36}$$

Assuming the energy of the orbital ψ_j to be ε_j, conservation of energy gives

$$k_f^2=\omega+\varepsilon_j . \tag{37}$$

By using the anti-Hermiticity of the gradient operator and neglecting unimportant constants the evaluation of Eq. (34) reduces to

$$\frac{d\sigma_j(\mathbf{k}_f)}{d\Omega}\sim\frac{k_f^3}{\omega}\left|\int\psi_j(\mathbf{r})e^{-i\mathbf{k}_f\cdot\mathbf{r}}d\mathbf{r}\right|^2 . \tag{38}$$

We will now restrict ourselves to polymers with pure translational symmetry but will at the end of this section relax this restriction. We can then write the initial wave function as

$$\psi_j(\mathbf{r})=(2M+1)^{-1/2}\sum_{n=-M}^{M}\sum_{\kappa\mathbf{R}L}\eta_{j\kappa\mathbf{R}L}e^{ik'nh}\chi_{\mathbf{R}nL\kappa}(\mathbf{r}) , \tag{39}$$

where a notation similar to that of Eqs. (18) and (19) has been adopted.

The orbital $\chi_{\mathbf{R}nL\kappa}$ is centered at $nh\hat{\mathbf{z}}+\mathbf{R}$. We therefore introduce

$$\mathbf{r}_{n\mathbf{R}}=\mathbf{r}-nh\hat{\mathbf{z}}-\mathbf{R} \tag{40}$$

and we can then write the partial photoelectron cross section per unit cell as

$$\frac{d\sigma'_j(\mathbf{k}_f)}{d\Omega}\sim\frac{k_f^3}{\omega}\left|(2M+1)^{-1/2}\sum_{n=-M}^{M}\sum_{\kappa\mathbf{R}L}\eta_{j\kappa\mathbf{R}L}e^{ik'nh}e^{-i\mathbf{k}_f\cdot(nh\hat{\mathbf{z}}+\mathbf{R})}\int\chi_{\mathbf{R}nL\kappa}(\mathbf{r}_{n\mathbf{R}})e^{-i\mathbf{k}_f\cdot\mathbf{r}_{n\mathbf{R}}}d\mathbf{r}_{n\mathbf{R}}\right|^2 . \tag{41}$$

Evaluation of this requires the useful expansion

$$e^{-i\mathbf{k}_f\cdot\mathbf{r}}=4\pi\sum_L i^{-l}j_l(k_fr)Y^*_L(\hat{\mathbf{r}})Y_L(\hat{\mathbf{k}}_f) . \tag{42}$$

Up to now the discussion has been general and as that of Mintmire and White.[16,51] We now specialize to the present LMTO method by inserting LMTO's as the basis functions χ. In evaluating the integrals in Eq. (41) we then notice that these can be simplified in the following way: For any system with more than one atom a LMTO centered at site $\mathbf{R}$ and having angular quantum numbers L does not have the pure symmetry about site $\mathbf{R}$ as described by L, since inside any other sphere it is augmented as described in Sec. II. We believe, however, that especially for large k_f for which $j_l(k_fr)$ [see Eq. (42)] is small and rapidly oscillating, ignoring the augmentation will lead to only modest errors. We accordingly approximate

$$\chi_{\mathbf{R}nL\kappa}(\mathbf{r})=\chi_{\mathbf{R}nL\kappa}(r)Y_L(\hat{\mathbf{r}}) , \tag{43}$$

which is to be valid for all r. Thus, $\chi_{\mathbf{R}nL\kappa}$ equals $\phi+\omega\dot{\phi}$ inside the sphere at $\mathbf{R}$ and a Hankel functions outside the sphere (i.e., also inside all other spheres).

Then Eq. (41) becomes

$$\frac{d\sigma'_j(\mathbf{k}_f)}{d\Omega}\sim\frac{k_f^3}{\omega}\left|\sum_{\kappa\mathbf{R}L}\eta_{j\kappa\tilde{\mathbf{R}}L}4\pi i^{-l}Y_L(\hat{\mathbf{k}}_f)e^{-i\mathbf{k}_f\cdot\mathbf{R}}\int_0^\infty r_{0\mathbf{R}}^2\chi_{\mathbf{R}0L\kappa}(\mathbf{r}_{0\mathbf{R}})j_l(k_fr_{0\mathbf{R}})dr_{0\mathbf{R}}(2M+1)^{-1}\sum_{n=-M}^{M}e^{inh(k'-\mathbf{k}_f\cdot\hat{\mathbf{z}})}\right|^2 . \tag{44}$$

The integrals in Eq. (44) can be evaluated as a sum of a numerical integral from 0 to $s_{\mathbf{R}}$, the sphere radius, and an analytical integral from $s_{\mathbf{R}}$ to ∞,

$$\int_0^\infty r^2\chi_{\mathbf{R}0L\kappa}(r)j_L(k_fr)dr=\int_0^{s_{\mathbf{R}}}r^2[\phi_{\mathbf{R}L}(r)+\omega^K_{\mathbf{R}L}(\kappa)\dot{\phi}_{\mathbf{R}L}(r)]j_l(k_fr)dr+\frac{i\kappa^{l+1}}{(2l-1)!!}c^K_{\mathbf{R}L}(\kappa)\int_{s_{\mathbf{R}}}^\infty r^2h_l^{(1)}(\kappa r)j_l(k_fr)dr \tag{45}$$

[cf. Eqs. (8) and (9)].

The angle-integrated spectrum

$$\sigma'_j(k_f)=\int\frac{d\sigma'_j(\mathbf{k}_f)}{d\Omega}d\Omega \tag{46}$$

can be calculated when approximating

$$(2M+1)^{-1}\sum_{n=-M}^{M} e^{inh(k'-\mathbf{k}_f\cdot\hat{\mathbf{z}})}\simeq 1 \tag{47}$$

which is valid for large M. Then

$$\sigma'_j(k_f)\sim\frac{k_f^3}{\omega}\sum_{\kappa_1\mathbf{R}_1L_1}\sum_{\kappa_2\mathbf{R}_2L_2}\gamma^*_{j\kappa_1\mathbf{R}_1L_1}\gamma_{j\kappa_2\mathbf{R}_2L_2}\int Y^*_{L_1}(\hat{\mathbf{k}}_f)Y_{L_2}(\hat{\mathbf{k}}_f)e^{i\mathbf{k}_f\cdot(\mathbf{R}_1-\mathbf{R}_2)}d\hat{\mathbf{k}}_f\ , \tag{48}$$

where

$$\gamma_{j\kappa\mathbf{R}L}=4\pi i^{-l}\eta_{j\kappa\mathbf{R}L}\int_0^\infty r^2\chi_{\mathbf{R}0L\kappa}(r)j_l(k_fr)dr\ . \tag{49}$$

Keeping the large-k_f approximation the integral in Eq. (48) is approximated through

$$\int Y^*_{L_1}(\hat{\mathbf{k}}_f)Y_{L_2}(\hat{\mathbf{k}}_f)e^{i\mathbf{k}_f\cdot(\mathbf{R}_1-\mathbf{R}_2)}d\hat{\mathbf{k}}_f\simeq\delta_{\mathbf{R}_1,\mathbf{R}_2}\delta_{L_1,L_2}\ , \tag{50}$$

which gives the final expression

$$\sigma'_j(k_f)\sim\frac{k_f^3}{\omega}\left|\sum_{\kappa\mathbf{R}L}\gamma_{j\kappa\mathbf{R}L}\right|^2 \tag{51}$$

with γ given by Eq. (49). We now notice that due to the approximation (50) we no longer need to restrict ourselves to polymers with translational symmetry, but can consider any screw-axis symmetry.

Finally, the total angle-integrated photoelectron spectrum is obtained by summing over all occupied orbitals j. Using Eq. (37) this results in a spectrum

$$\sigma(\varepsilon)=\sum_{j=1}^{\text{occ}}\sigma'_j(k_f)\Big|_{k_f^2=\omega+\varepsilon_j}\cdot\delta(\varepsilon-\varepsilon_j) \tag{52}$$

which is a density-of-state curve modulated by matrix-element effects.

For the periodic polymers the summation over occupied orbitals involves an integration over the Brillouin zone (20) and for each k point a summation over the occupied orbitals. In any practical calculation the continuous k variable is replaced by a discrete set $\{0=k_1<k_2<\cdots<k_{N_K-1}<k_{N_K}=1\}$. As a one-dimensional analog to the tetrahedral method used for evaluation of a density of states for three-dimensional periodic structures,[53] we will write the density of states $D(\varepsilon)$ as well as the photoelectron spectra $\sigma(\varepsilon)$ as functions that are piecewise constant. E.g., denoting the jth eigenvalue for the ith k point ε_{ji}, we will approximate the density of states of the jth band $D_j(\varepsilon)$ with

$$D_j(\varepsilon)=\sum_{i=1}^{N_K-1}D_{ji}(\varepsilon)\ ,$$

$$D_{ji}(\varepsilon)=\begin{cases}2\left|\dfrac{k_{i+1}-k_i}{\varepsilon_{j,i+1}-\varepsilon_{ji}}\right| & \text{for } \min\{\varepsilon_{ji},\varepsilon_{j,i+1}\}<\varepsilon\le\max\{\varepsilon_{ji},\varepsilon_{j,i+1}\}\\ 0 & \text{otherwise}\ ,\end{cases} \tag{53}$$

and equivalent for $\sigma(\varepsilon)$. We have included the factor 2 to account for spin degeneracy and have accordingly no spin polarization. It should be added that in order to be able to distinguish between allowed and avoided band crossings it is important to have a proper description of the symmetries of the orbitals, such that no extra peaks appear in the calculated spectra and none are omitted.

For the sake of completeness we finally mention that a simplified method for calculating the photoelectron spectra is often applied. In that method the direct evaluation of the matrix elements is avoided. It is instead based on the Mulliken gross populations as, e.g., described in Sec. V but separated into angular components. For each orbital the photoelectron cross section is then calculated by summing the populations times the corresponding cross sections for the free atoms.[54]

B. *Trans*-polyacetylene

In Fig. 3(a) we show our calculated total density of states for the optimized structure of *trans*-polyacetylene. The figure is directly comparable with the energy bands of Fig. 2. In Figs. 3(b) and 3(c) we show the separate contributions from the σ and the π bands, respectively. In order to get more smooth curves they have been broadened by Gaussians of FWHM $=0.5$ eV (full width at half maximum).

Equivalent to Fig. 3 we show in Fig. 4 the calculated x-ray photoemission spectroscopy (XPS) spectra (photon energy $=100$ a.u.$=1.36$ keV) and in Fig. 5 the calculated ultraviolet photoemission spectroscopy (UPS) spectra (3 a.u.$=41$ eV), which also have been split into σ and π

electron contributions. In Figs. 4 and 5 we have arbitrarily set the energy origin at the top of the valence bands.

Comparison between Figs. 4 and 5 demonstrates the well known fact that XPS has the largest cross sections for orbitals with large s components (i.e., in the lower part of the spectra of Fig. 4), whereas UPS is more sensitive to p-like orbitals.

Mintmire *et al.*[16,51,55] have presented theoretical XPS spectra. Their spectra are dominated by peaks at -17 and -10 eV with smaller peaks at -13 and -5 eV. Of those, that at -10 eV is a double peak. Except for a constant shift of 1 eV (see below), these features are all found in Fig. 4(a). Mintmire *et al.* show that their spectra agree well with experimental ones by Brundle[56] and since the alignment of the spectra is related with some uncertainty, we conclude that our XPS spectra in Fig. 4 are realistic.

Also UPS spectra were reported by Mintmire *et al.*[16,51,55] Here, the dominant features appear at -10 and -5 eV with smaller extra peaks at -8 and -1 eV. The last peak must be due to the upper edge of the π valence bands, which in Figs. 4 and 5 per definition have placed at 0. This therefore accounts for the above-mentioned 1-eV difference between our XPS spectra and those of Mintmire *et al.* With this difference in mind we notice a good agreement between Fig. 5(a) and the spectra of Mintmire *et al.*

There exists more experimental UPS spectra[57–60] of which those by Rasmusson *et al.*[60] are both the most recent and the most detailed ones. Relative to the top of the valence bands their spectra indicate peaks at -16, -10, -7, and -4 eV, which are seen to be in perfect agreement with our calculated spectra in Fig. 5. The older spectra do not differ in any significant features from those of Rasmusson *et al.*

In total we find that we can calculate the photoelectron spectra accurately. *Trans*-polyacetylene is structurally so simple that an interpretation of the spectra is not too complicated, and we have therefore omitted it here. But for more complicated polymers it becomes more difficult to interpret the experimental spectra and, as demonstrated here, the present calculational scheme should be able to assist in the interpretation.

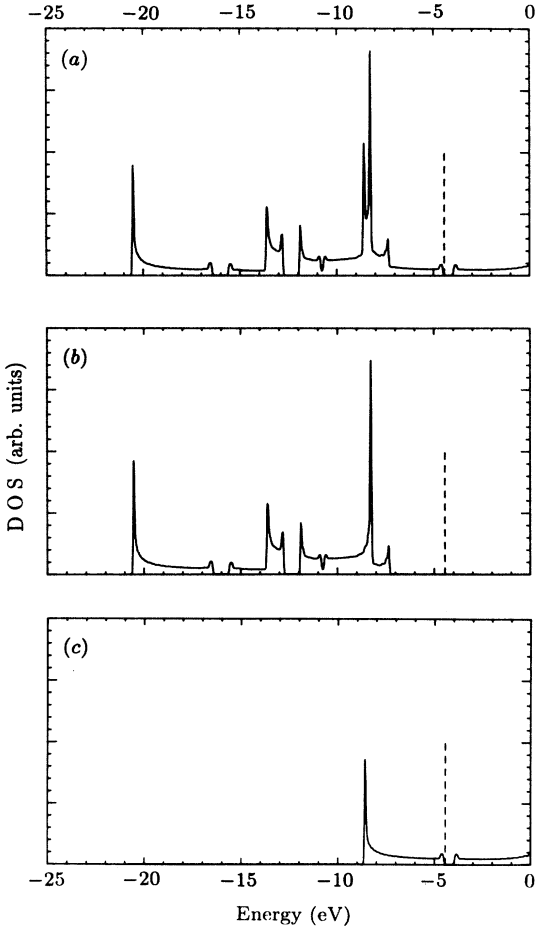

FIG. 3. (a) Total, (b) σ, and (c) π electron density of states. The curves have been broadened by Gaussians of width 0.5 eV. The vertical dashed lines represent the top of the valence bands.

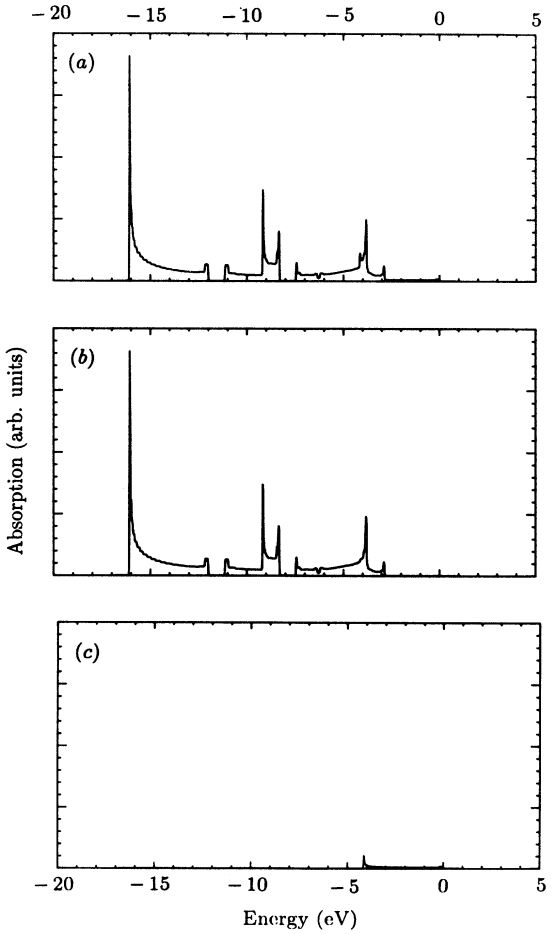

FIG. 4. Calculated photoelectron spectra for photon energies of 1.36 keV (corresponding to XPS). The top of the valence bands has been chosen as energy origin, but otherwise the figure corresponds to Fig. 3.

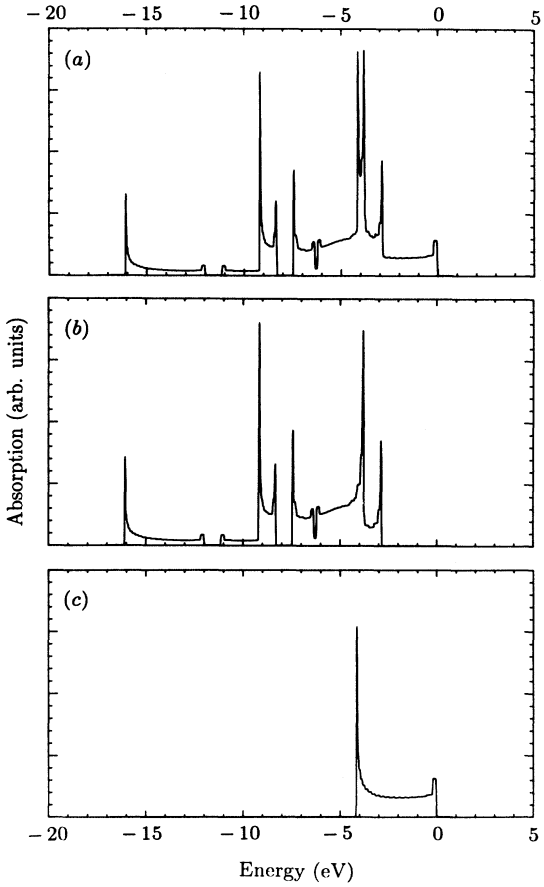

FIG. 5. As Fig. 4, but for photon energies of 41 eV (UPS).

VII. ELECTRON-ENERGY-LOSS SPECTRA

A. A qualitative loss function

The self-consistent, longitudinal, dielectric function is given by[16,61–64]

$$\epsilon_L(\mathbf{q},\omega)=1+\frac{8\pi}{q^2V}\sum_{jj'\mathbf{k}}\frac{|(j\mathbf{k}|j',\mathbf{k}+\mathbf{q})|^2}{\hbar\omega+\varepsilon_{j\mathbf{k}}-\varepsilon_{j',\mathbf{k}+\mathbf{q}}}\times[f_0(\varepsilon_{j',\mathbf{k}+\mathbf{q}})-f_0(\varepsilon_{j\mathbf{k}})]\ , \quad (54)$$

where j and j' are band indices, $\mathbf{k}$ is the crystal momentum, V is the volume per unit cell, and $f_0(\varepsilon)$ is the Fermi-Dirac distribution function which at zero temperatures is 0 (1) for $\varepsilon>\varepsilon_F$ ($\varepsilon<\varepsilon_F$). Finally,

$$(j\mathbf{k}|j',\mathbf{k}+\mathbf{q})=\frac{1}{V}\int_{\text{u.c.}}\psi^*_{j\mathbf{k}}(\mathbf{r})e^{-i\mathbf{q}\cdot\mathbf{r}}\psi_{j',\mathbf{k}+\mathbf{q}}(\mathbf{r})d\mathbf{r}\ , \quad (55)$$

where "u.c." means integration over one unit cell.

The loss function is given by[64]

$$S_L(\mathbf{q},\omega)=\lim_{\delta\to0}\text{Im}\{[\epsilon_L(\mathbf{q},\omega+i\delta)]^{-1}\} \quad (56)$$

which upon insertion in Eq. (54) gives for $T=0$

$$S_L(\mathbf{q},\omega)=\frac{8\pi^2}{q^2V}\sum_{jj'\mathbf{k}}|(j\mathbf{k}|j',\mathbf{k}+\mathbf{q})|^2|f_0(\varepsilon_{j\mathbf{k}})-f_0(\varepsilon_{j',\mathbf{k}+\mathbf{q}})|\times\delta(\omega+\varepsilon_{j\mathbf{k}}-\varepsilon_{j',\mathbf{k}+\mathbf{q}})\ . \quad (57)$$

Thus, compared with the scattering processes of the preceding section which involved such large excitation energies that the scattered electrons could be considered as free electrons, the excitations here involve valence- to conduction-orbital transitions with relatively small energy differences. Therefore, for extended periodic systems the photoelectron spectra will essentially give information about the valence density of states (D_v), whereas the loss spectra give information about convolutions of D_v with the conduction density of states (D_c). A simple approximation to the loss function is thus to assume it a modulation of

$$P_L(\mathbf{q},\omega)=\sum_{jj'\mathbf{k}}|f_0(\varepsilon_{j\mathbf{k}})-f_0(\varepsilon_{j',\mathbf{k}+\mathbf{q}})|\delta(\omega+\varepsilon_{j\mathbf{k}}-\varepsilon_{j',\mathbf{k}+\mathbf{q}})\ . \quad (58)$$

For the quasi-one-dimensional polymers with translational (not helical) symmetry we will therefore study the function $P_L(q,\omega)$, where the k values of conduction and valence orbitals differ by $\pm q$. In this approximation we have neglected matrix-element effects and examine accordingly only the q-dependent joint density of states. As a comparison between Figs. 3, 4, and 5 demonstrates, a similar approximation for the optical spectra gives qualitatively good results for *trans*-polyacetylene, and we believe therefore the approximation to be justified. However, only single-particle excitations are thereby included, and plasmon peaks will be lacking in our calculated electron-energy-loss spectra.

Finally, in the discussion above nowhere have we made use of our specific LMTO basis set. Similar procedures can therefore be carried through for any other method, too.

B. *Trans*-polyacetylene

For highly crystalline samples one may experimentally distinguish between transitions from valence orbitals (v) of either σ or π symmetry to conduction orbitals (c) of either σ or π symmetry. Using a notation of the form $v\to c$ this leaves us with four possible types of transitions: $\sigma\to\sigma$, $\sigma\to\pi$, $\pi\to\sigma$, and $\pi\to\pi$. Since for each value of q we would therefore have four spectra, we have chosen to limit the presentation of the results to those of Fig. 6. This figure shows the calculated onsets (solid curves) and the calculated positions of the peaks (dashed curves) in the spectra as functions of q for the four different types of transitions.

As is well known conduction bands from density-functional calculations with a local-density approximation are less accurate than valence bands. The results of Fig. 6 must therefore be taken with some caution. Therefore, the $\pi\to\pi$ transitions, which are those that have been most extensively discussed in the literature, appear at too low energies, which is most obvious for $q=0$ where the onset should appear at the position of the optical gap.

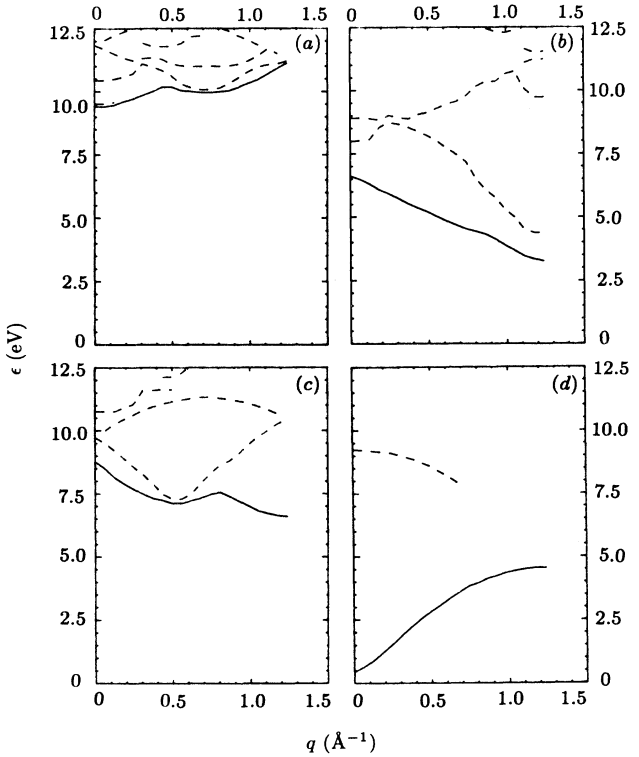

FIG. 6 Calculated onsets (solid curves) and maxima (dashed curves) for valence- to conduction- ($v \rightarrow c$) band transitions as functions of momentum transfers. The transition types are (a) $\sigma \rightarrow \sigma$, (b) $\sigma \rightarrow \pi$, (c) $\pi \rightarrow \sigma$, and (d) $\pi \rightarrow \pi$.

Fink and co-workers[65,66] have reported $\pi \rightarrow \pi$ onsets starting at 1.5–2.0 eV for $q=0$ and raising approximately linearly as a function of q with a slope of about 6 eV Å. A maximum (corresponding to a collective π plasmon) appears at 4.5 eV for $q=0$ and increases with a slope of about 3.3 eV Å. Whereas our calculated slope of the onset agrees with that of Fink and co-workers[65,66] the maximum has not been caught by our simple model which only includes single-particle or band excitations, but has been obtained in the more accurate study of Mintmire and White.[16,63] Fink and co-workers[65,66] also observed a peak at 12 eV for $q=0$ which they ascribed a $\sigma \rightarrow \sigma$ transition in agreement with Fig. 6(a) and with the results of Mintmire and White.[16,63] Finally, Fink and co-workers[65,66] noticed features at about 7 eV for small q, which they could not explain. We suggest (see Fig. 6) these to be related to $\sigma \rightarrow \pi$ excitations.

VIII. MOMENTUM DENSITIES

A. Theory

In Compton scattering high-energy photons are scattered inelastic from a sample. For a given scattering angle information about the momentum distribution of the electrons in the sample is obtained from an analysis of the energy of the scattered photons. For disordered samples only spherically averaged momentum distributions can be extracted, but for crystalline samples information about angular dependencies can be obtained. Since the core electrons are delocalized in momentum space and the valence electrons more localized, this experimental technique is particularly useful in deriving information about the valence electrons and hence about chemical bonds (see, e.g., Ref. 67).

A theoretical study of Compton scattering must accordingly start with a calculating of the wave functions in momentum space. Using Eq. (13) we thus must calculate with the present LMTO method

$$\begin{aligned}\varphi_j(\mathbf{p}) &= (2\pi)^{-3/2}\int e^{-i\mathbf{p}\cdot\mathbf{r}}\psi_j(\mathbf{r})d\mathbf{r} \\ &= (2\pi)^{-3/2}\sum_{RL}\left[a_{jRL}\int_{\mathrm{MTS}} e^{-i\mathbf{p}\cdot\mathbf{r}}\phi_{RL}(\mathbf{r}_R)d\mathbf{r} + b_{jRL}\int_{\mathrm{MTS}} e^{-i\mathbf{p}\cdot\mathbf{r}}\dot{\phi}_{RL}(\mathbf{r}_R)d\mathbf{r}\right] \\ &\quad + (2\pi)^{-3/2}\sum_{\kappa RL} d_{j\kappa RL}\int_{\mathrm{IR}} e^{-i\mathbf{p}\cdot\mathbf{r}}K_{RL}(\kappa;\mathbf{r}_R)d\mathbf{r}\ , \end{aligned} \tag{59}$$

where the integrals labeled "MTS" are over the muffin-tin spheres and those labeled "IR" are over the interstitial region.

Denoting the radius of the muffin-tin sphere at site $\mathbf{R}$, s_R we have thus to evaluate muffin-tin-sphere integrals of the type

$$\begin{aligned}\int e^{-i\mathbf{p}\cdot\mathbf{r}}\breve{\phi}_{RL}(\mathbf{r}_R)\Theta(|\mathbf{r}-\mathbf{R}|-s_R)d\mathbf{r} &= e^{-i\mathbf{p}\cdot\mathbf{R}}\int e^{-i\mathbf{p}\cdot\mathbf{r}_R}\breve{\phi}_{RL}(\mathbf{r}_R)\Theta(\mathbf{r}_R-s_R)d\mathbf{r}_R \\ &= e^{-i\mathbf{p}\cdot\mathbf{R}}\int e^{-i\mathbf{p}\cdot\mathbf{r}}\breve{\phi}_{RL}(\mathbf{r})\Theta(r-s_R)d\mathbf{r}\ , \end{aligned} \tag{60}$$

where $\breve{\phi}$ is either ϕ or $\dot{\phi}$, and $\Theta(x)$ is a step function which is 1 (0) for $x<0$ ($x>0$).

By using Eq. (42), Eq. (60) reduces to

$$\sqrt{2/\pi}e^{-i\mathbf{p}\cdot\mathbf{R}}(-i)^l Y_L(\hat{\mathbf{p}})\int_0^{s_R} r^2\breve{\phi}_{RL}(r)j_l(pr) \equiv \breve{\varphi}_{RL}(\mathbf{p})\ , \tag{61}$$

since

$$\breve{\phi}_{RL}(\mathbf{r}) = \breve{\phi}_{RL}(r)Y_L(\hat{\mathbf{r}}) \tag{62}$$

for $r < s_{\mathbf{R}}$.

The interstitial integrals in Eq. (59) are calculated using Eq. (10),

$$(2\pi)^{-3/2}\int_{\mathrm{IR}} e^{-i\mathbf{p}\cdot\mathbf{r}}K_{\mathbf{R}L}(\kappa;\mathbf{r}_{\mathbf{R}})d\mathbf{r}=(2\pi)^{-3/2}\int_{|\mathbf{r}-\mathbf{R}|>s_{\mathbf{R}}} e^{-i\mathbf{p}\cdot\mathbf{r}}K_{\mathbf{R}L}(\kappa;\mathbf{r}_{\mathbf{R}})d\mathbf{r}$$

$$-(2\pi)^{-3/2}\sum_{\mathbf{R}'\neq\mathbf{R}}\sum_{L'}S_{LL'}(\kappa;\mathbf{R}-\mathbf{R}')\int_{|\mathbf{r}-\mathbf{R}'|<s_{\mathbf{R}'}} e^{-i\mathbf{p}\cdot\mathbf{r}}J_{\mathbf{R}'L'}(\kappa;\mathbf{r}_{\mathbf{R}'})d\mathbf{r}'$$

$$=\sqrt{2/\pi}e^{-i\mathbf{p}\cdot\mathbf{R}}(-i)^l Y_L(\hat{\mathbf{p}})\int_{s_{\mathbf{R}}}^{\infty} r^2 K_{\mathbf{R}L}(\kappa;r)j_l(pr)dr$$

$$-\sqrt{2/\pi}\sum_{\mathbf{R}'\neq\mathbf{R}} e^{-i\mathbf{p}\cdot\mathbf{R}'}\sum_{L'}(-i)^{l'}Y_{L'}(\hat{\mathbf{p}})S_{LL'}(\kappa;\mathbf{R}-\mathbf{R}')\int_0^{s_{\mathbf{R}'}} r^2 J_{\mathbf{R}'L'}(\kappa;r)j_{l'}(pr)dr\ ,$$

where we have made use of Eqs. (10) and (42).

The functions $\phi_{\mathbf{R}L}$ and $\dot{\phi}_{\mathbf{R}L}$ are represented numerically inside the muffin-tin spheres. The integrals in Eq. (61) are therefore to be evaluated numerically, which subsequently means that we have to represent the eigenfunctions in momentum space numerically. Since the Fourier transformation in Eq. (59) should not change the normalization, we can use the normalization as a measure for the precision of the evaluation of Eq. (59). We will here summarize our thereby obtained experience.

In evaluating Eqs. (61) and (63) one should use the formulas as they are, and accordingly not apply Eq. (42) in expanding the exponentials. Such an expansion could otherwise lead directly to an appealing form of $\varphi_j(\mathbf{p})$ like

$$\varphi_j(\mathbf{p})=\sum_L \varphi_{jL}(p)Y_L(\hat{\mathbf{p}})\ , \tag{64}$$

which can be obtained by writing the products of two spherical harmonics as a linear combination of single spherical harmonics. It turns out, however, that the internal summations leading to Eq. (64) become very slowly converging.

The one-dimensional integrals in Eq. (63) can easily be evaluated analytically, whereas those of Eq. (61) are to be calculated numerically. For large p the integrand oscillates rapidly, which may lead to numerical errors. We circumvented this problem by writing the integrand as a smooth term (which in turn was assumed linearly varying between the points in which it was given) times a rapidly oscillating part of the form $\cos(pr)$ and/or $\sin(pr)$. These expressions could then be integrated analytically in each small interval between neighboring points in the radial mesh.

Depending on the problem we have used 100–200 p points logarithmically distributed in the interval 0.1 a.u. $\leq p \leq$ 120 a.u. Moreover, we used between 20 and 100 directions $\hat{\mathbf{p}}$.

After having calculated $\varphi_j(\mathbf{r})$ as described above we are left with the function values in a large number of $\mathbf{p}$ points. We then seek an expansion of the form (64). This is done by making a least-squares fit to the form (64) for each fixed value of $p=|\mathbf{p}|$.

We finally obtain the density by using

$$\rho_j(\mathbf{r})=|\varphi_j(\mathbf{p})|^2=\left|\sum_L \varphi_{jL}(p)Y_L(\hat{\mathbf{p}})\right|^2$$

$$\equiv\sum_L \rho_{jL}(p)Y_L(\hat{\mathbf{p}})\ , \tag{65}$$

and by summing over the occupied orbitals (over j) we find the total density.

For the polymers (for which we will restrict ourselves to translational symmetry) an additional problem shows up. The momentum representation of the Bloch wave of Eq. (18) is ($\hat{\mathbf{z}}$ is a unit vector in the z direction)

$$\chi^k_{\mathbf{R}L\kappa}(\mathbf{p})=(2M+1)^{-1/2}(2\pi)^{-3/2}\sum_{n=-M}^{M} e^{in\pi k}\int\chi_{\mathbf{R}nL\kappa}(\mathbf{r})e^{-i\mathbf{p}\cdot\mathbf{r}}d\mathbf{r}$$

$$=(2M+1)^{-1/2}(2\pi)^{-3/2}\sum_{n=-M}^{M}\left[e^{in\pi k}\int\chi_{\mathbf{R}0L\kappa}(\mathbf{r}-nh\hat{\mathbf{z}})e^{-i\mathbf{p}\cdot\mathbf{r}}d\mathbf{r}\right]$$

$$=(2M+1)^{-1/2}(2\pi)^{-3/2}\sum_{n=-M}^{M}\left[e^{in\pi k}e^{-ip_z nh}\int\chi_{\mathbf{R}0L\kappa}(\mathbf{r})e^{-i\mathbf{p}\cdot\mathbf{r}}d\mathbf{r}\right]$$

$$=\left[(2M+1)^{-1/2}\sum_{n=-M}^{M} e^{in(\pi k-p_z h)}\right]\left[(2\pi)^{-3/2}\int\chi_{\mathbf{R}0L\kappa}(\mathbf{r})e^{-i\mathbf{p}\cdot\mathbf{r}}d\mathbf{r}\right] \tag{66}$$

(see, e.g., Ref. 68). In the limit of large M the first factor vanishes unless

$$\pi k - p_z h = n' 2\pi \tag{67}$$

with n' an integer, and for those values the function diverges (see Ref. 68). This means that an expansion of form (64) or (65) is meaningless. But, if we integrate over a whole band [i.e., over the Brillouin zone (20)], the resulting density becomes a smooth function of p_z, since for any value of p_z there exists a $k \in [-1,1]$ for which Eq. (67) is satisfied. Since in any actual calculations we are forced to have a finite, discrete set of k values, numerical problems may influence the results especially when the character of the band orbitals is rapidly changing as a function of k, as, e.g., is the case near an avoided crossing. As we shall see for *trans*-polyacetylene, this can lead to errors of the order of 10% in the calculated momentum densities. Our experience has shown that these inaccuracies are essentially absent for finite molecules and for polymers consisting of weakly interacting units. This supports our suggestion of relating them to bands of rapidly changing character as a function of k and also suggests that the total momentum density is more accurate than those of single bands.

In closing this section we mention that some of these problems may be circumvented by using Wannier functions instead of Bloch waves. We have not examined this here. A more fundamental problem is whether one can use the density-functional orbitals in studying momentum distributions. Lam and Platzman[69] have discussed this and also proposed an improvement. We have chosen here to ignore the problems, as has often been done (for a further discussion, see, e.g., Refs. 70–73). It should finally be added that some of the numerical problems mentioned in this section also occur for the calculation of the photoelectron spectra, especially for large photon energies. They will, however, be less noticeable there.

B. *Trans*-polyacetylene

We calculated the momentum densities for the optimized structure of *trans*-polyacetylene. In order to limit the above-mentioned numerical problems we used 21 equally spaced k points in the interval between (and including) $k=0$ and 1. In Fig. 7 we show the results.

The σ_1 band [Fig. 7(a)] has the main contributions for small p. Especially the p_z component is localized to small-p values. The normalization gives 1.03 (instead of 1). The σ_2 and σ_3 bands show a pronounced avoided crossing (see Fig. 2) and the corresponding momentum densities are therefore related with uncertainties of about 10%. Both momentum densities [Figs. 7(b) and 7(c)] show maxima for p_z close to 1 and p_x slightly smaller, which are at slightly larger p values for the σ_3 band than for the σ_2 band. We believe this similarity to be a consequence of the avoided crossing, such that the character of the orbitals of one band for a part of the Brillouin zone is close to that of the orbitals of the other band for the remaining part of the Brillouin zone. The density of the σ_4 band is more accurately calculated than those of the σ_2 and σ_3 bands. It shows [Fig. 7(d)] a characteristic two-peak structure for the p_z component.

Finally, the simple variation of the π_1 orbitals as function of k makes the calculation of the density of this band the most accurate of them all. The density has vanishing p_x and p_z components, and it shows a maximum for $p_y \simeq 0.55$ a.u. [see Fig. 7(e)].

The total density in momentum space is shown in Fig. 7(f) and is that which will be most easily accessible in a Compton-scattering experiment. It is normalized to 10.5 instead of 10 indicating a total 5% error. Except for a peak for the p_z component for $p_z \simeq 0.65$ a.u. it is very structureless. Since the length of the unit cell is 4.788 a.u., standing waves are expected for $p_z = n\pi/h = n(0.656$ a.u.), with n an integer. This explains the local maximum for the p_z component.

IX. THE RECIPROCAL FORM FACTOR

A. Theory

As exemplified above for *trans*-polyacetylene, the total momentum density is very structureless and there is actually only a small difference between that of a compound and the sum of those of the consistent free atoms. But, Fourier transforming the momentum density gives a function in position space $B(\mathbf{r})$ which has been demonstrated to be very useful in studying Compton scattering, especially when the argument $\mathbf{r}$ is comparable with interatomic distances.[67,74,75] This so-called reciprocal form factor is accordingly for the jth orbital defined as

$$B_j(\mathbf{r}) = \int \rho_j(\mathbf{p}) e^{-i\mathbf{p}\cdot\mathbf{r}} d\mathbf{p} , \tag{68}$$

and it can be shown[67,75] that $B_j(\mathbf{r})$ is an autocorrelation function in position space,

$$B_j(\mathbf{r}) = \int \chi_j(\mathbf{s}) \chi_j^*(\mathbf{r}+\mathbf{s}) d\mathbf{s} . \tag{69}$$

$B_j(\mathbf{r}=\mathbf{0})$ is therefore equal to 1. Moreover, when integrating over a whole band for a periodic system, the corresponding reciprocal form factor will vanish whenever $\mathbf{r}$ is a lattice vector.

In calculating $B_j(\mathbf{r})$ we have chosen to start with the angular expansion of Eq. (65). Using Eq. (42) we then immediately arrive at

$$B_j(\mathbf{r}) = \sqrt{2/\pi} \sum_L i^l Y_L(\hat{\mathbf{r}}) \int_0^\infty p^2 j_l(pr) \rho_{jL}(p) dp \tag{70}$$

in which we can evaluate the integral numerically since $\rho_{jL}(p)$ is given numerically.

An alternative procedure has been proposed by Rozendaal[76] in which one avoids direct calculation of the functions in momentum space but arrives at a closed expression for $B_j(\mathbf{r})$ involving the wave function in position space. This is done by starting with Eq. (59) directly, squaring, and Fourier transforming under application of Eq. (42) several times. We have, however, found that for systems with more than very few atoms some of the many summations are so slowly converging that a calculation becomes prohibitively expensive or inaccurate.

B. *Trans*-polyacetylene

In Fig. 8 we show the reciprocal form factors for *trans*-polyacetylene corresponding to the momentum densities of Fig. 7. We have only focused on the regions for $|r|>3$ a.u., since below this r value the function only raises steeply towards either 1 (the reciprocal form factor for the single bands) or the number of valence electrons (the total reciprocal form factor). That the z components do not vanish for $z=n(4.788$ a.u.) is a consequence of the numerical problems discussed in the preceding section, but it is seen to be best fulfilled for the σ_1 and the π_1 bands.

The best interpretation of the curves is obtained by using Eq. (69) and thus consider the x, y, and z components of $B_j(\mathbf{r})$ as the overlap between an orbital and itself displaced parallel with the x, y, or z, axis, respectively. In particular the x and y components of the reciprocal form factors for the individual bands are then readily understood.

Finally, the large difference in the z component and the other two in Fig. 8(f) suggests that the total $B(\mathbf{r})$ (which is the function it is easiest to extract from an experiment) can be used as an experimental tool in quantifying chain alignment in a sample. The Compton-scattering experiment using high-energy photons is only slightly sensitive to surface effects and defects, such that these will not obscure the interpretation significantly.

X. A MODEL FOR *TRANS*-POLYACETYLENE

A. The model

We will now describe a model which we will use in the following section in studying solitons and polarons. The model is closely related to the SSH model described in the Introduction, but modified in order to account for the results of our first-principles calculations on periodic

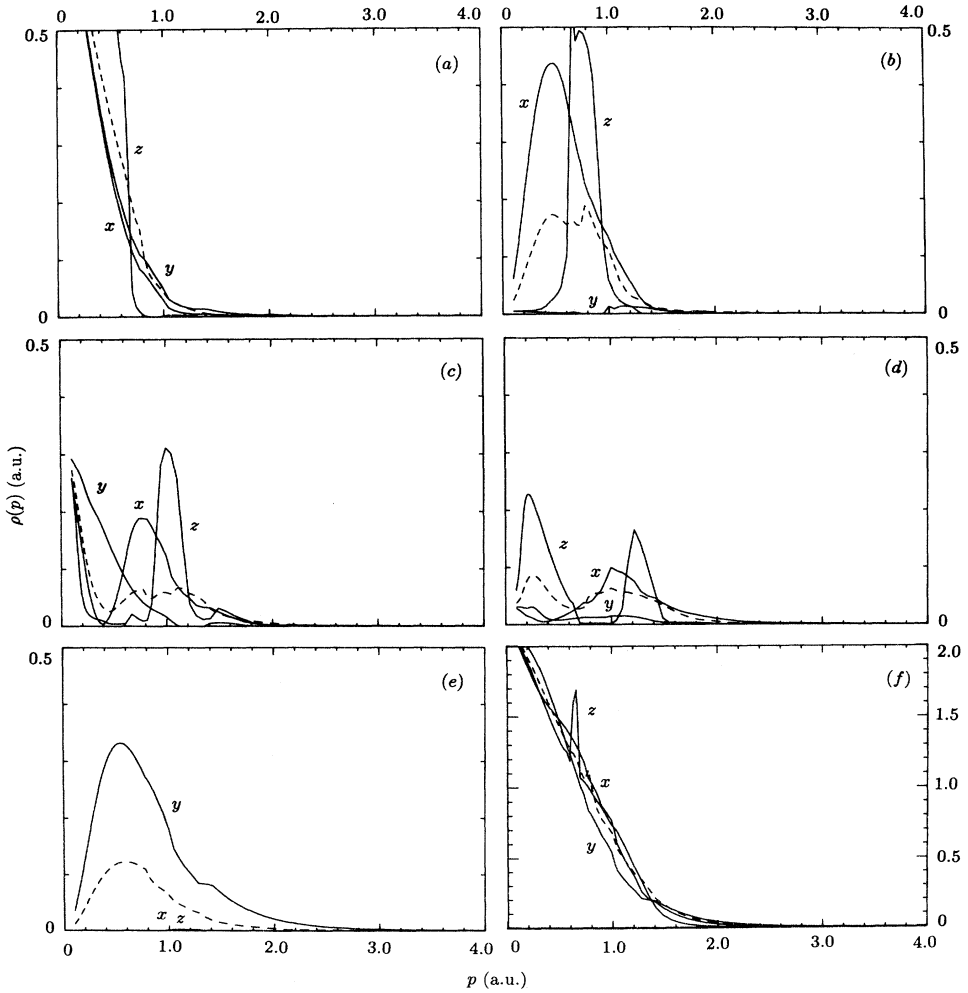

FIG. 7. The momentum densities for *trans*-polyacetylene. The polymer is assumed placed in the (x,z) plane with the z axis parallel with the polymer axis. x, y, and z label the p_z, p_y, and p_z components, respectively, and the dashed line is the spherical average. The densities are for (a) the σ_1 band, (b) the σ_2 band, (c) the σ_3 band, (d) the σ_4 band, and (e) the π_1 band. (f) shows the total density.

chains. As the SSH model it is a single-particle model and accordingly does not include many-body terms as given in, e.g., (extended) Hubbard models or PPP (Pariser-Parr-Pople) models. Since, however, many-body effects are included in the first-principles calculations, the mapping of the results on a single-particle model means that some many-body effects are included through renormalized single-particle interactions.

As demonstrated in Secs. IV and V, the frontier orbitals of *trans*-polyacetylene are π orbitals centered almost exclusively on the carbon atoms. These orbitals will be described with a tight-binding Hamiltonian,

$$\hat{H}_\pi = \sum_{n,s} \varepsilon_n c^\dagger_{n,s} c_{n,s} - \sum_{n,s} \sum_{m=1}^{2} t_{n,n+m} (c^\dagger_{n,s} c_{n+m,s} + c^\dagger_{n+m,s} c_{n,s}) \ . \quad (71)$$

Here, n is a carbon site index, s a spin variable, and $c^\dagger_{n,s}$ and $c_{n,s}$ the creation and annihilation operators, respectively, of a π electron on site n with spin s. Moreover, ε_n and $t_{n,n+m}$ are the on-site terms and the hopping integrals, respectively. Compared with the original SSH model,[34,35] $\hat{H}_\pi$ of Eq. (71) is generalized by direct inclusion of the on-site terms, which, moreover, may be site dependent, and by the next-nearest-neighbor hopping integrals (i.e., $m=2$).

Contour plots of the electron densities of the π valence orbitals for $k=0$ and 1 have shown[18] that the hydrogen atoms do play a role, but the Mulliken populations of Sec. V demonstrated that this is in fact minor, such that a model with only one orbital per CH unit seems justified.

Following Su, Schrieffer, and Heeger, we introduce configuration coordinates $\{u_n\}$. u_n is the displacement of the nth carbon atom parallel to the polymer axis relative to its position for the hypothetic periodic structure with vanishing bond-length alternation; see Fig. 9. For the periodic structure with alternating bond lengths we have

$$u_n = (-1)^n u_0 \ . \quad (72)$$

We will denote the distance (bond length) between atom n and atom $n+m$, $d_{n,n+m}$. For the structure (72) with $u_0=0$ all nearest-neighbor bond lengths are identical ($=d_0$). For $u_n \ll d_0$ the distance becomes

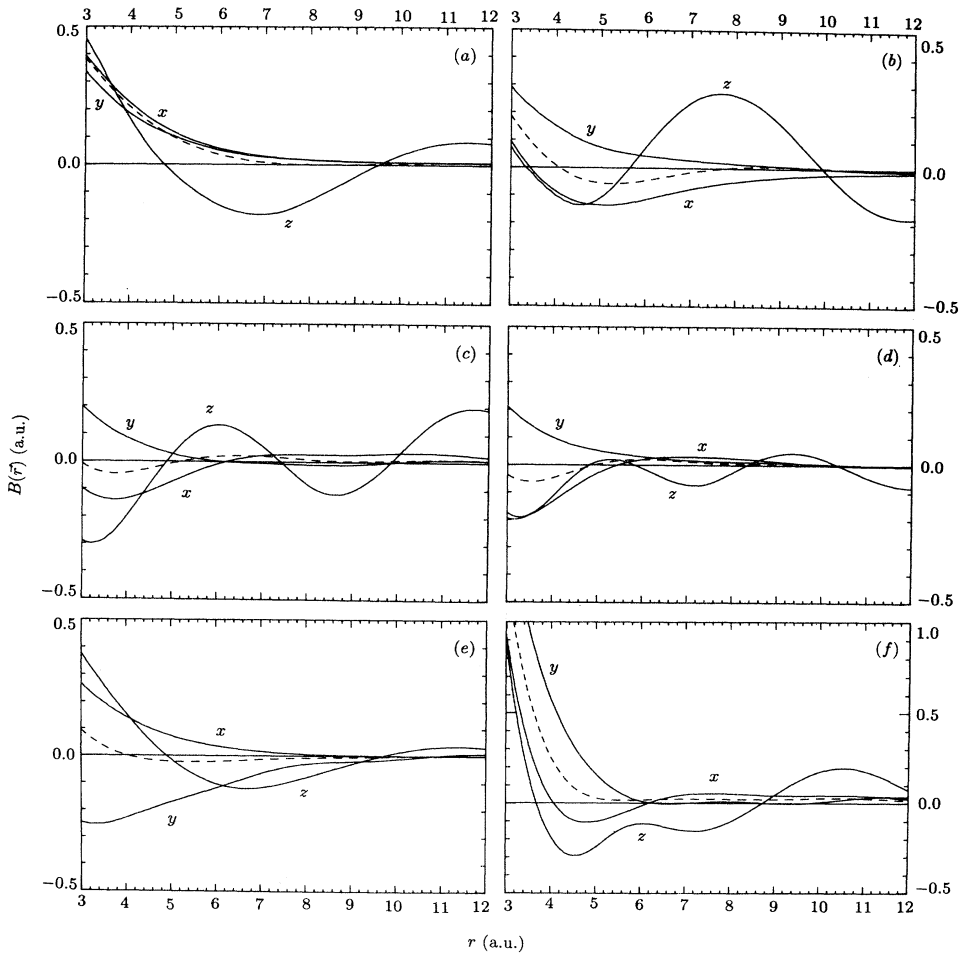

FIG. 8. The reciprocal form factor $B(\mathbf{r})$ equivalent to the results of Fig. 7. x, y, and z label $\mathbf{r}$ along the x, y, or z axis, respectively.

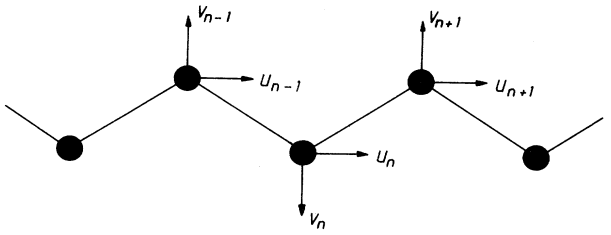

FIG. 9. The configuration coordinates u_n and v_n which describe the position of the nth carbon atom.

$$d_{n,n+1} \simeq d_0 + (u_{n+1} - u_n)\sin(\beta/2) ,$$
$$d_{n,n+2} = 2d_0 \sin(\beta/2) + (u_{n+2} - u_n) , \tag{73}$$

with β being the C—C—C bond angle. (We have here assumed the parameters v_n of Fig. 9 to vanish, as will be discussed in Sec. X B.)

Like Su, Schrieffer, and Heeger, we write the hopping integrals as linear functions of the bond lengths and using Eq. (73) we have

$$t_{n,n+m} = t_m^{(0)} - \alpha_m (u_{n+m} - u_n) . \tag{74}$$

For the periodic structures of Figs. 1(a) and 1(b) all on-site terms ε_n must be identical. However, using Fig. 1(c) as a reference, we notice that the carbon atom with only single bonds as the bonds to its two nearest carbon neighbors can be considered "unsaturated" and will attract extra electrons. Also for solitons spread out over more sites there will be partly "unsaturated" carbon atoms. The tendency to attract extra electrons can be modeled through bond-length-dependent variations in ε_n,

$$\begin{aligned} \varepsilon_n &= \varepsilon_0 - \zeta'[(d_{n,n+1} - d_0) + (d_{n-1,n} - d_0)] \\ &\simeq \varepsilon_0 - \zeta' \sin(\beta/2)[(u_{n+1} - u_n) + (u_n - u_{n-1})] \\ &= \varepsilon_0 - \zeta(u_{n+1} - u_{n-1}) , \end{aligned} \tag{75}$$

where we have made use of Eq. (73). In order to determine $\hat{H}_\pi$ completely we thus need six parameters: $t_1^{(0)}$, $t_2^{(0)}$, α_1, α_2, ε_0, and ζ.

That part of the total Hamiltonian which is not included in $\hat{H}_\pi$ is written as a simple function of $\{u_n\}$. Whereas the SSH model includes only the simplest harmonic terms, we will also include anharmonic terms. Thus,

$$\begin{aligned} \hat{H}_\sigma &\equiv \hat{H}_{\text{tot}} - \hat{H}_\pi \\ &= \tfrac{1}{2} K_2 \sum_n (u_{n+1} - u_n)^2 + \tfrac{1}{4} K_4 \sum_n (u_{n+1} - u_n)^4 . \end{aligned} \tag{76}$$

The six parameters of $\hat{H}_\pi$ and the two of $\hat{H}_\sigma$ (i.e., K_2 and K_4) are now to be determined from the first-principles calculations on periodic chains as will be discussed in Sec. X B.

B. The perfect chain

We will ultimately be interested in chains in which we have inserted a soliton or a polaron. It must be assumed that the generation of a soliton or a polaron will not change the total length of the polymer. We therefore considered periodic chains in which the unit-cell length was fixed at the optimized value reported in Sec. III. Moreover, in the first-principles calculations we fixed the positions of the hydrogen atoms as described in Sec. III. We are then left with two geometrical parameters to vary (see Fig. 9): the displacements u_n parallel to the polymer axis obeying Eq. (72), and the displacements v_n perpendicular to the polymer axis. For the periodic chains the latter are defined to obey

$$v_n = v_0 \tag{77}$$

with $v_0 = 0$ for the optimized structure. The first-principles calculations were then performed for various values of (u_0, v_0).

The shift $u_0 \rightarrow -u_0$ corresponds to passing from the one bond-length alternation to the other, i.e., from the structure of Fig. 1(a) to that of Fig. 1(b). The first-principles calculations for this transition demonstrated that the smallest variations in the total energy were obtained when keeping $v_0 = 0$. In that case we found the total-energy variations shown in Fig. 10 where we show the energy as a function of bond-length alternation defined as

$$\Delta d = d_{2n-1,2n} - d_{2n,2n+1} = 4 \sin(\beta/2) u_0 , \tag{78}$$

where we have used Eq. (73).

The key quantity in Fig. 10 is—besides the size of the bond-length alternation—the dimerization energy E_{dim}, which is defined as the total energy per CH unit of the undimerized structure minus that of the optimized (dimerized) structure. From Fig. 10 we see that we find $E_{\text{dim}} = 0.028$ eV.

There exist various other theoretical estimates for E_{dim} obtained with different methods and/or restrictions in the

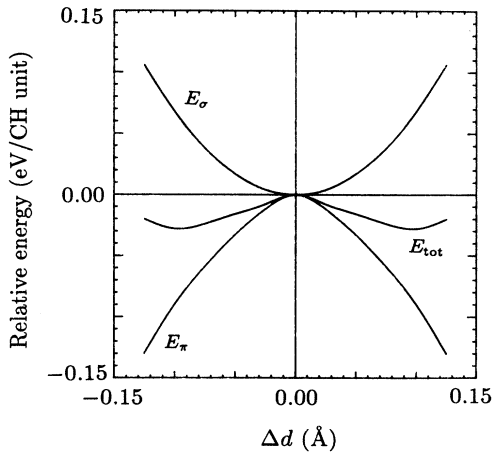

FIG. 10. Relative total energy (E_{tot}), the π-electron single-particle energy (E_π), and the difference ($E_\sigma \equiv E_{\text{tot}} - E_\pi$) in eV per CH unit as functions of the difference in the nearest-neighbor bond lengths Δd for periodic chains. The results have been obtained from the first-principles calculations.

geometry variations. We will here discuss some of those.

First of all, Su, Schrieffer, and Heeger[34,35] predicted $E_{\rm dim}=0.015$ eV as a result of their model which was parametrized in order to reproduce the experimental value of Δd and of the gap. Another semiempirical calculation but using the CNDO (complete neglect of differential overlap) method[77] predicted $E_{\rm dim}=0.079$ eV.

The *ab initio* Hartree-Fock calculations by Kertész, Koller, and Ažman[78] and by Suhai[79] were performed on only one dimerized and one undimerized structure. Also they gave large values of $E_{\rm dim}$: $E_{\rm dim}=0.15$ eV by Kertész, Koller, and Ažman and 0.18 eV by Suhai. Much more detailed studies were undertaken by Karpfen and Petkov[3,4] and Karpfen and Höller,[5] who optimized the structure in more detail for both the dimerized and the undimerized form. The difference in the total energies for the two isomers give $E_{\rm dim}=0.11$ eV using a small basis set[3] and $E_{\rm dim}=0.034$ eV with an improved basis set.[4] For an even more detailed geometry optimization but with the smaller basis set later calculations increased $E_{\rm dim}$ to 0.16 eV.[5]

Finally, Suhai[8,9] has performed a detailed study using extended basis sets and also including a perturbational treatment of correlation effects. He demonstrated that improved basis sets led to reductions in $E_{\rm dim}$, which for the best basis set was reported to be 0.076 eV. Correlation effects reduced this further to 0.043 eV. Similar results have recently been obtained by König and Stollhoff[14] who found $E_{\rm dim}=0.06$ eV without correlation and $E_{\rm dim}=0.04$ eV when including correlation.

A restricted density-functional study by Mintmire and White[15,16] gave, on the other hand, a small $E_{\rm dim}$: $E_{\rm dim}=0.016$ eV, whereas one of us with a very limited geometry variation found $E_{\rm dim}=0.12$ eV.[17,18] In contrast to this, the density-functional calculations on crystalline *trans*-polyacetylene by Ashkenazi *et al.*[19,28] have all predicted a very small dimerization energy: $E_{\rm dim}=0.003$ eV (Ref. 19) or $E_{\rm dim}=0$.[22,28]

With few exceptions all calculations predict $E_{\rm dim}$ to be larger than found by Su, Schrieffer, and Heeger.[34,35] This means that unless the values of the parameters of the $\hat{H}_\pi$ model Hamiltonian differ significantly from those proposed by SSH, one has to include anharmonic terms in $\hat{H}_\sigma$, e.g., by allowing K_4 in Eq. (76) to be different from zero.[80]

Since the valence energies are well reproduced by the density-functional calculations, we can use the integral over the π_1 valence band as obtained in our first-principles calculations to give the π contribution to the total energy. This contribution, labeled E_π, is also shown in Fig. 10. The difference $E_{\rm tot}-E_\pi$ is then per definition the σ contribution, which is to be described by $\hat{H}_\sigma$ of Eq. (76). Also this, labeled E_σ, is shown in Fig. 10.

We can use the two different total-energy expressions of Sec. III to obtain more information about the contents of Fig. 10. Using e_1 of Eq. (30) our calculations show that the contributions from the nonspherical parts of the potential and charge density inside the muffin-tin spheres are important. That term is lowered with 0.047 eV per CH unit when passing from the undimerized structure to the dimerized structure. This does, however, not necessarily mean that a set of self-consistent calculations with only spherically symmetric components inside the muffin-tin spheres will predict the structure with vanishing bond-length alternation to have the lowest total energy. E_0 of Eq. (31) is upon dimerization lowered by 0.19 eV per CH unit, which is the double of the lowering in E_π of Fig. 10, also indicating that the σ-band energies are lowered upon dimerization. This was also found in an earlier study, but for a much more limited geometry variation.[17,18] It is, however, *not* to be interpreted as saying that the σ electrons prefer a dimerized structure, since in the first-principles calculations all electrons interact with each other.

Some of the parameters of $\hat{H}_\pi$ of Eq. (71) can now be determined from the π_1 valence bands for different values of Δd (or, equivalently, u_0). We find with the values of SSH in parentheses: $\varepsilon_0=-4.36$ ($-$) eV, $t_1^{(0)}=2.45$ (2.5) eV, $\alpha_1=6.36$ (4.1) eV/Å, and $t_2^{(0)}=-0.12$ ($-$) eV. Neither α_2 nor ζ could be determined in this set. Since, however, the effects of the next-nearest-neighbor interactions are small,[81] we have chosen to ignore the effects of α_2, i.e., to set $\alpha_2=0$.

We determined ζ by looking at the π_1 valence band for structures with $u_n=u_0=0$ but $v_n=v_0>0$. This corresponds to increasing all bond lengths simultaneously by $2v_0\cos(\beta/2)$ for $v_0\ll d_0$. For an overall lowering in the π_1 valence energies of $\Delta\varepsilon$, we can use Eq. (75) in obtaining

$$\Delta\varepsilon=\zeta'\times 2v_0\cos(\beta/2)=\zeta\times 2v_0\cot(\beta/2)$$
$$\Longrightarrow\zeta=\frac{\Delta\varepsilon}{2v_0}\tan(\beta/2)\ . \qquad (79)$$

Our calculations resulted in $\zeta=8.85$ eV/Å.

The lowest total energy in our calculations was found for $u_0=u_{(0)}=0.028$ Å, whereas SSH forced their parameters to give $u_{(0)}=0.040$ Å. Therefore, although our α_1 value is significantly larger than the SSH value, the nearest-neighbor hopping integrals become almost identical in the two models for the optimized structure. Moreover, as discussed elsewhere,[18] the α_1 value of SSH is smaller than usually assumed for hydrocarbons. We finally mention that for a very localized soliton as that schematically shown in Fig. 1(c), ε_n of the site of the soliton is lowered by $\zeta\times 2u_{(0)}=0.5$ eV.

Choosing $K_4=0$ in Eq. (76), the (approximately) right ground-state structure is found for $K_2=48.5$ eV/Å^2. This is to be compared with the SSH value of 21 eV/Å^2, but here the difference in $u_{(0)}$ can also be held responsible for the difference. However, only for $K_4\neq 0$, the right $E_{\rm dim}$ can be obtained, and realistic values are then $K_2=30.5$ eV/Å^2 and $K_4=7339$ eV/Å^4.

König and Stollhoff[14] have used their *ab initio* Hartree-Fock results in estimating $\alpha_1=4.0$ eV/Å and $K_2=30$ eV/Å^2. Their value of $u_{(0)}$ is slightly larger than ours: $u_{(0)}=0.033$ Å. On the other hand, the earlier limited LMTO calculations on more compact chains (the C—C—C bond angles were kept at 120°) predicted

$t_1^{(0)}=3.78$ eV, $\alpha_1=5.45$ eV/Å, and $t_2^{(0)}=0.38$ eV.[17,18] We find in total that our present values are more realistic and in better accord with other sets of parameter values.

Since our model differs in several aspects from the original SSH model we have chosen to study models with five different parameter sets. Thereby we could gradually modify the SSH model such that it ultimately (for the last parameter set) becomes our own model, and could examine the effects of each modification separately. $\hat{H}_\pi$ and $\hat{H}_\sigma$ were defined as in Eqs. (71) and (76), respectively, but the parameter values differed. In the first set we used the values of SSH. In the second set we used our values but with $t_2^{(0)}=\zeta=K_4=0$ (and therefore $K_2=48.5$ eV/Å^2). The third set was obtained by including the proper $t_2^{(0)}$ value, and in the fourth set we also used the correct K_2 and K_4 values. Our full parameter set was used in the fifth and last set. In all sets (including the first) we used $\varepsilon_0=-4.36$ eV.

In Fig. 11 we show for comparison the relative energies for the first [Fig. 11(a)], the second and third [Fig. 11(b)], and the fourth and fifth [Fig. 11(c)] sets for the periodic chains as functions of u_0. Since $t_2^{(0)}$ and ζ do not affect these results, the results for the second and the third and those for the fourth and the fifth set are pairwise identical. The results were obtained considering a ring molecule with $N=200$ sites. We thereby avoid end effects and impose periodic boundary conditions.

The SSH parameters give a total-energy minimum [Fig. 11(a)] for $u_0=u_{(0)}=\pm 0.040$ Å. The other sets give minima close to the value we found in the first-principles calculations, i.e, $u_0=u_{(0)}=\pm 0.029$ Å in Fig. 11(b) and $u_0=u_{(0)}=\pm 0.026$ Å in Fig. 11(c). The dimerization energy is calculated to be 0.013, 0.018, and 0.028 eV, respectively. It is remarkable that $\partial^2 E_{\rm tot}/\partial u_0^2|_{u_0=u_{(0)}}$ are similar in Figs. 11(a) and 11(b) (33 and 40 eV/Å^2, respectively), but, on the other hand, significantly larger in Fig. 11(c) (237 eV/Å^2). However, by including even one more term in $\hat{H}_\sigma$, the curvature can also be given any desired value without changing $u_{(0)}$ or $E_{\rm dim}$.

We performed one more calculation for the optimized structure of each model but with $N=700$. The resulting density of states were broadened with Gaussians of FWHM=0.05 eV and are shown in Fig. 12 for the first parameter set [Fig. 12(a)] and the last set [Fig. 12(b)]. The curves are seen to be very similar; the largest difference being that the valence band in Fig. 12(b) is narrower than the conduction band due to the next-nearest-neighbor interactions.

In comparing Fig. 12(b) with the results of the first-principles calculations, we notice first of all that the gap in Fig. 12(b) is much more realistic than that of the first-principles calculations, which may be accidental. A more careful inspection of Figs. 12(b) and 3(a) reveals that especially the top of the valence band and the bottom of the conduction band is shifted more away from the Fermi level in the model calculations than in the first-principles calculations. Since we are essentially interested in those orbitals this is a weakness of the present model. This may be related to the use of a finite (6 for $k\in[0;1]$) number of k points in the first-principles calculations. In Ref. 39 it was argued that for linear carbon chains, E_π would be reduced by something like 30% when passing from 6 to an infinite number of k points. However, also with such a reduction, *trans*-polyacetylene is found to dimerize. We have chosen to ignore these problems and use the model above, since it has the appealing feature of giving a realistic gap. When appropriate we will discuss some of the implications of a modified model. Finally, the valence band of Fig. 12(b) is slightly too narrow, whereas the conduction band is too broad, indicating that our value of $t_2^{(0)}$ is too large.

Since we have included neither interchain interactions nor many-body effects, we stress that the model is not perfect, but should represent a very realistic single-particle approximation to *trans*-polyacetylene. We will now in the next section use the model in studying solitons and polarons.

XI. SOLITONS AND POLARONS IN *TRANS*-POLYACETYLENE

A. Solitons

Su, Schrieffer, and Heeger[34,35] proposed a soliton as schematically shown in Fig. 1(c) to be modeled through

$$u_n=(-1)^n u_0 \tanh(n/L)\ , \tag{80}$$

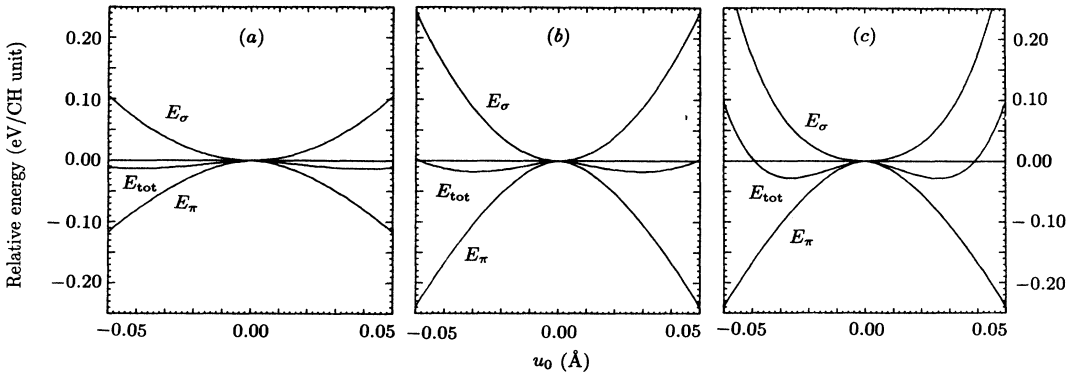

FIG. 11. As Fig. 10 but obtained from model calculations and as functions of u_0. In (a) we use the SSH parameters, in (b) and (c) the present ones. Only harmonic terms in $\hat{H}_\sigma$ are used in (b), whereas $\hat{H}_\sigma$ is anharmonic in (c).

where the center of the soliton is supposed at $n=0$. It has later been shown[82] that Eq. (80) is the exact form in the continuum limit of the SSH model.

For a ring molecule with an even number N at sites one has to introduce solitons in pairs. With N large and even we will accordingly generalize Eq. (80) to

$$u_n=(-1)^n u_0 \tanh\left[\frac{n+\delta+\Delta}{L}\right]\tanh\left[\frac{n+\delta-\Delta}{L}\right], \quad (81)$$

where 2Δ is the distance between the soliton and the antisoliton. Moreover, δ is a parameter that can be varied in order to model the propagation of the soliton-antisoliton pair. With $2\Delta=N/2$ the distance between the soliton and the antisoliton becomes largest possible, and for N sufficiently large they will not interact.

We have used the model described in the preceding section with the five different parameter sets. It turned out that the results were almost independent of δ (indicating the solitons to be highly mobile), and we will therefore focus on the results for $\delta=0$. Furthermore, we set $u_0=u_{(0)}$ and $2\Delta=N/2$. We then only have L to vary. We optimized L for doubly positively or negatively charged ring molecules ["doubly," since the chain contains two (anti)solitons], as well as for a neutral, but spin-containing ring molecule. The charge and/or spin is varied by varying the occupation of the orbitals closest to the Fermi level. In the discussion below we will define the binding energy E_b as the negative of the total energy of the soliton-containing chain minus that of the undistorted chain of the same charge and spin. And since we have two solitons we will divide by 2 in order to get the energy per soliton. The creation energy of a singly charged, undistorted chain equals the energy of the top of the valence bands (the bottom of the conduction bands) for positive (negative) chains, and E_b can therefore also be interpreted as the lowering in creation energy of charged chains due to soliton formation. For an undistorted chain with a spin, the creation energy equals the gap and the binding energy can be interpreted in the same way.

For the first parameter set (that of SSH) we found $L=7.9$ independent of charge and spin. We found $E_b=0.25$ eV for the charged chains and $E_b=0.90$ eV for the spin-containing chain. The soliton induces a gap state which is placed exactly at midgap [see Fig. 13(a)], as is well known.

Very similar results were found for the second set. L was optimized to be 6.5, the binding energies were 0.27 eV for charged solitons and 1.01 eV for the spin soliton. Here the gap state is also at midgap (i.e., at -4.36 eV).

Introducing next-nearest-neighbor interactions (third parameter set) leads to a small difference in positively and negatively charged solitons: $L=6.4$ and 6.7 for the two, respectively. Moreover, $E_b=0.28$ and 0.27 eV in the two cases, respectively. For the spin soliton the situation is unchanged from that of the second parameter set. As

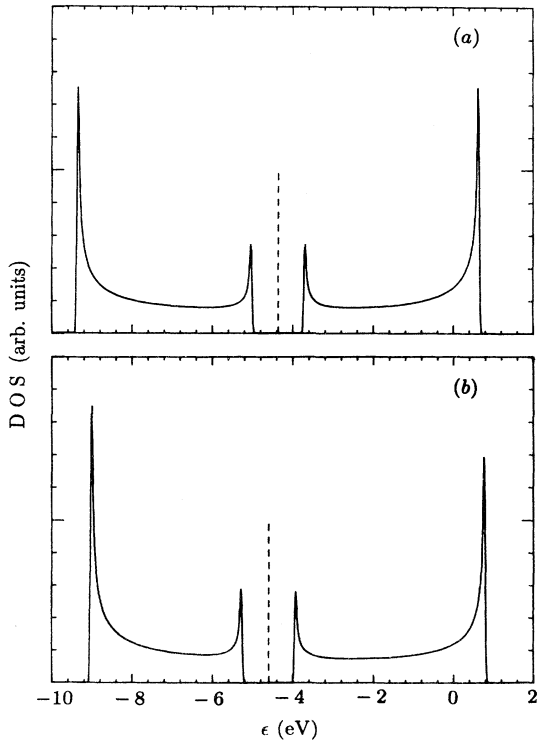

FIG. 12. The π-electron density of states obtained in the model calculations for the perfect optimized chain. The vertical dashed line is the Fermi level for the neutral system. In (a) we have used the SSH parameters, in (b) the present ones.

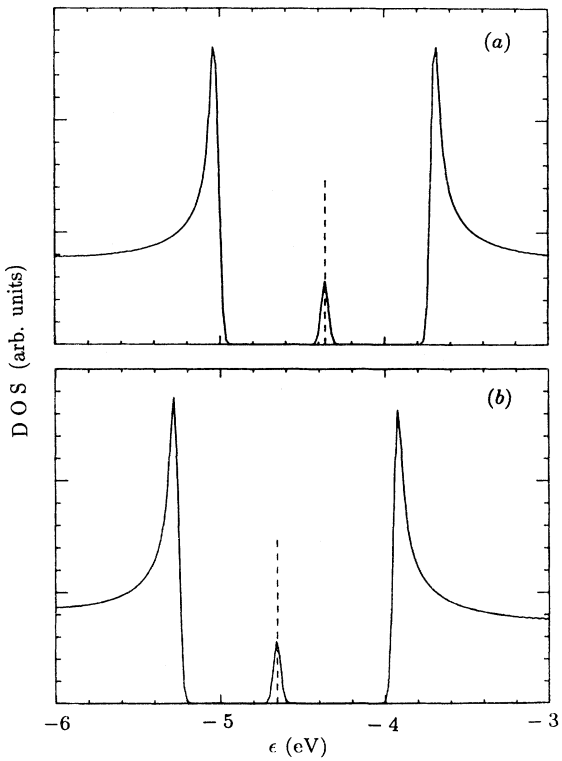

FIG. 13. The π-electron density of states obtained in the model calculations for the chain with a soliton. The vertical dashed line is the Fermi level for the neutral system. In (a) we have used the SSH parameters, in (b) the present ones. Only the part closest to the Fermi level is shown.

demonstrated elsewhere[81] next-nearest-neighbour interactions lead to a very small shift of the gap state away from the midgap position.

Increasing the dimerization energy by setting $K_4 \neq 0$ as in the fourth parameter set leads to some changes. L is roughly halved being 3.2 for positively and 3.3 for negatively charged solitons, and 3.2–3.3 for the spin soliton. Also the binding energies are decreased, being 0.16, 0.15, and 0.81 eV in the three cases. As for the third parameter set, the gap states appear close to midgap.

When we introduce $\zeta \neq 0$ as in our final (fifth) parameter set, important modifications show up. There is a clear difference in the optimized L values, which become 3.9, 1.6, and 2.8 for the positive, negative, and spin soliton, respectively. The binding energies are 0.10, 0.14, and 0.83 eV, respectively. The effect of ζ is obviously to attract extra electrons, which explains the large difference in E_b for positive and negative solitons. Finally, the gap is between -5.28 and -3.92 eV [see Fig. 13(b)], such that the midgap position is at -4.60 eV. However, the soliton-induced states now appear at -4.66, -4.68, and -4.67 eV, respectively. Thus, a shift towards the valence-band edge is observed [see Fig. 13(b)], which intuitively can be expected since the atoms near the center of the solitons have lower on-site energies due to $\zeta \neq 0$.

In comparing our results with those of others it should be mentioned that there exists a vast literature on model calculations on *trans*-polyacetylene (see, e.g., Refs. 2, 37, and 38), and it is impossible to give proper reference to all. We will therefore here only consider some few relevant papers.

The most important finding in our model calculations with our (fifth) parameter set is that we—using a physically well-founded single-particle model—find soliton-induced states shifted noticeably away from the midgap position. We believe this shift to remain approximately constant also when using a model that gives a smaller dimerization energy. The main difference will then be an increase in the optimized values of L. Baeriswyl, Campbell, and Mazumdar[83] have shown that for a SSH model extended with a Hubbard-U term one gets a shift [of about $U/(3L)$] of the gap level, but that this shift is towards the valence-band edge for the charged solitons and towards the conduction-band edge for the spin soliton. In our model the shift is always towards the valence-band edge. Thus, a comparison of experimental results on neutral and charged polyacetylene could offer a possibility to separate the two effects. It does, however, also mean that the shift towards the valence-band edge observed for charged polyacetylene does *not* necessarily indicate a Hubbard U different from 0.

Sum, Fesser, and Büttner[84] have also demonstrated that an extended single-particle SSH model may lead to soliton states away from the midgap position. They, however, have not offered any physically intuitively clear explanation of their extra terms.

Parameter-free calculations have been performed on soliton-containing chains. Both density-functional calculations on infinite chains[85] and on finite molecules,[86] as well as *ab initio* Hartree-Fock calculations on finite molecules[87] predict the soliton-induced levels to appear asymmetric in the gap.

Optical experiments have been performed both on doped[88–91] and on photoexcited[92,93] polyacetylene. For the doped samples an absorption at 0.65–0.75 eV is observed, whereas the absorption is at 0.5 eV for the photoexcited samples. Thus, in all cases the absorption is closer to the valence-band edge in agreement with our findings. However, the shift from midgap is about twice what we predict, and the remainder may thus be ascribed to many-body effects. Combining our results with those of Baeriswyl, Campbell, and Mazumdar,[83] this finally suggests that the Hubbard U is only half so large as usually proposed, when basing the proposal on photoabsorption data.

For the sake of completeness we finally mention that Fu *et al.*[94] in their model calculations have observed more soliton-induced states outside the band regions. We do not observe similar features.

In Fig. 14 we show the wave functions of the soliton-induced gap states, in Fig. 14(a) using the original SSH parameters and in Fig. 14(b) using our parameters. We notice that the wave functions are very similar although the L values are very different. As pointed out elsewhere[81] the width of the orbital does not need to follow the width of the lattice distortion, and Fig. 14 represents clearly an example for this. This further means that ENDOR (electron nuclear double resonance) experiments on neutral but spin-containing samples are to be inter-

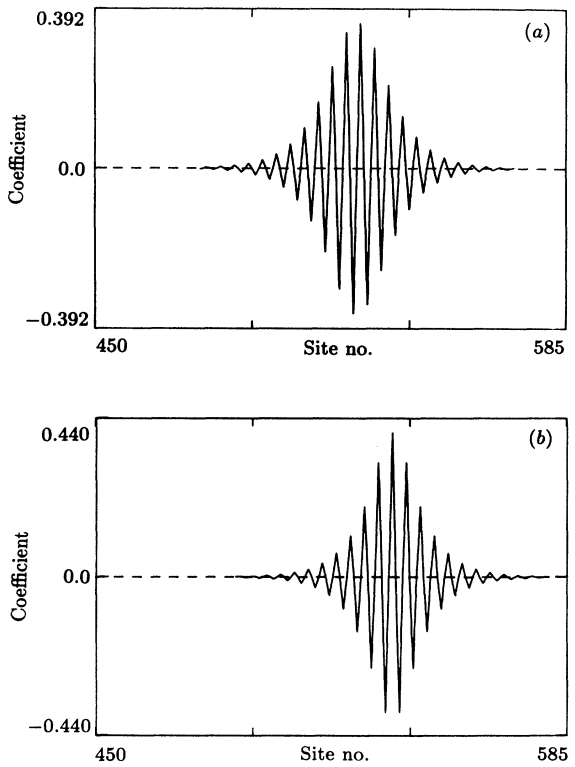

FIG. 14. The wave function of one of the gap states in Fig. 13. Shown are the coefficients to the different carbon p functions as a function of carbon site. (a) and (b) correspond to the two cases in Fig. 13.

preted as only giving information on the wave functions and not on the lattice distortion.

Finally, the next-nearest-neighbor interactions lead to small components on the "odd" sites between the large components seen in Fig. 14 on the "even" sites. These components are, however, only few percents of the large components.

B. Polarons

When we reduce Δ in Eq. (81), the soliton and the antisoliton start to interact and ultimately they may form a bound pair, the polaron.[95–98] For small Δ one may replace Eq. (81) by

$$u_n=(-1)^n u_0\left[1-\alpha\,\mathrm{sech}\left[\frac{n+\delta+\Delta}{L}\right]\times\mathrm{sech}\left[\frac{n+\delta-\Delta}{L}\right]\right]. \quad (82)$$

We will here only consider the form (82). As a consequence of the formation of the polaron, the two gap levels interact and split into a bonding and an antibonding combination.

We only considered two parameter sets, the first and the last, i.e., the original due to Su, Schrieffer, and Heeger and the most detailed present one. For the SSH set we found optimized polarons for charged chains with one electron added or removed and for chains with the spin of one electron reversed. The optimized values were $\Delta=3.0$, $L=11.0$, and $\alpha=0.7$. The binding energies were 0.075 eV for the charged chains and 0.29 eV for the spin-containing chain. The gap levels appear symmetric in the gap [see Fig. 15(a)] about 0.22 eV from the band edges. The corresponding orbitals of the two gap levels are very similar, and in Fig. 16(a) we show that of the lower level, which is seen to resemble the superposition of two soliton functions.

On the contrary, we believe that our own model does not support polarons. The gap levels [see Fig. 15(b)] appear very close (<0.02 eV) to the band edges and the orbitals [Fig. 16(b)] are so delocalized that finite-size effects become noticeable, and we believe that the polaronic distortions will ultimately disappear for very long chains.

In Ref. 34 it was shown how an improved SSH model for linear carbon chains (polyyne) with anharmonic terms in $\hat{H}_\sigma$ led to a preference of polarons over solitons for chains with nonzero charge or spin. There, both the σ energy and the π energy each favored the structure with $u_n=u_0=u_{(0)}$ over that with $u_n=u_0=0$. Here for *trans*-polyacetylene, the σ energy favors the undimerized structure slightly over the dimerized structure. We believe

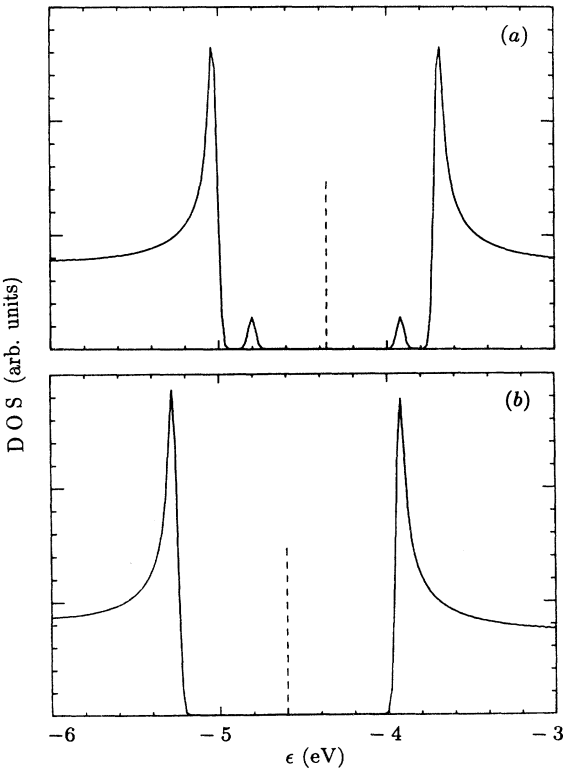

FIG. 15. The π-electron density of states obtained in the model calculations for the chain with a polaron. The vertical dashed line is the Fermi level for the neutral system. In (a) we have used the SSH parameters, in (b) the present ones. Only the part closest to the Fermi level is shown.

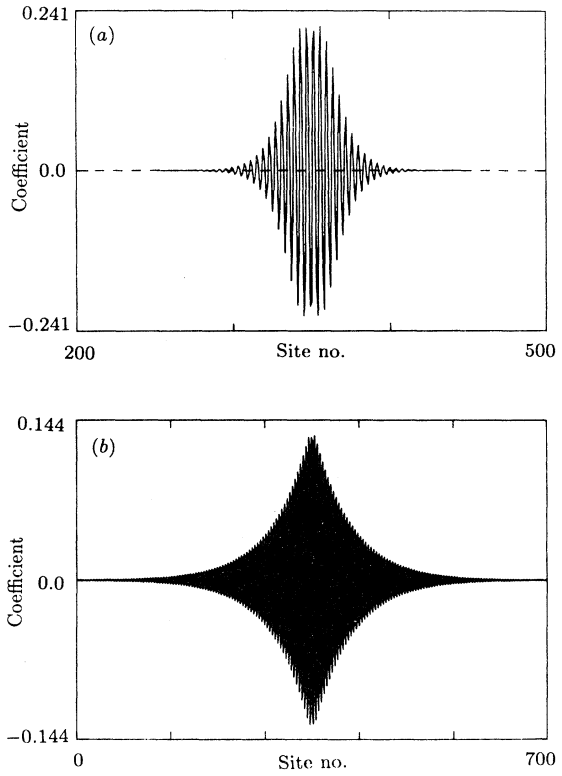

FIG. 16. The wave function of the lowest gap state in Fig. 15. Shown are the coefficients to the different carbon p functions as a function of the carbon site. (a) and (b) correspond to the two cases in Fig. 15.

this difference to be the main reason for the difference in relative energies of solitons and polarons. It may therefore be slightly modified when using a model which predicts a smaller dimerization energy, but we believe that solitons will remain the stabler distortions.

XII. CONCLUSIONS

The aim of the present paper has been twofold. First of all we have presented a detailed theoretical study of the electronic properties of *trans*-polyacetylene. Second, we have shown how the first-principles, density-functional, full-potential LMTO method for helical polymers may be extended in order to calculate various experimentally accessible quantities.

We first demonstrated that one may introduce two different expressions for the total energy when using the density-functional formalism. These are in principle identical, but approximations in any actual calculation make them differ. The difference can be used as an estimate of the quality of the calculations. Having established well-converged calculations we subsequently demonstrated that our method predicted the lowest total energy for neutral periodic *trans*-polyacetylene for a structure with a nonvanishing C—C bond-length alternation. Whereas this agrees with experimental findings and results of *ab initio* Hartree-Fock calculations and of density-functional calculations on single chains, it contrasts recent findings of Ashkenazi *et al.*,[22] who used another density-functional method. We argued, however, that their results might be due to three-dimensional effects, although the mechanism behind the bond-length alternation cannot be considered fully understood.

In subsequent sections we showed that the calculated band structures were to be considered very realistic. We also demonstrated how photoelectron spectra and information about electron-energy-loss spectra could be calculated, and that these agreed well with available experimental findings for *trans*-polyacetylene. Moreover, we presented a method for calculating momentum-space properties, which are of relevance for Compton scattering experiments. The results for *trans*-polyacetylene suggested Compton scattering to be an experimental method for studying the degree of chain alignment in the sample.

Mulliken populations demonstrated that the frontier orbitals of *trans*-polyacetylene mainly are formed by carbon p orbitals. We used this and other findings of the first-principles calculations in deriving a modified SSH model for *trans*-polyacetylene. This model contains next-nearest-neighbor interactions and an "ionicity" term in the π part as well as anharmonic terms in the σ part.

We finally used the model in studying solitons and polarons. Polarons were found to be unstable, and the soliton-induced gap states were found to be placed asymmetric in the gap shifted towards the valence-band edge. This latter is in agreement with experimental results, and suggests that a Hubbard U is smaller than often assumed. Moreover, the width of the solitonic orbitals was larger than the width of the underlying lattice distortion, and the solitons were slightly different for chains of different charge and/or spin.

ACKNOWLEDGMENT

The work was supported by the Swedish National Board for Technical Development within the framework of ESPRIT Basic Research Action 3314.

[1]C. K. Chiang, C. R. Fincher, Jr., Y. W. Park, A. J. Heeger, H. Shirakawa, E. J. Louis, S. C. Gau, and A. G. MacDiarmid, Phys. Rev. Lett. **39**, 1098 (1977).
[2]Proceedings of the International Conference on Science and Technology of Synthetic Metals, Santa Fe, 1988 [Synth. Met. **27-29** (1988–1989)].
[3]A. Karpfen and J. Petkov, Solid State Commun. **29**, 251 (1979).
[4]A. Karpfen and J. Petkov, Theor. Chim. Acta (Berlin) **53**, 65 (1979).
[5]A. Karpfen and R. Höller, Solid State Commun. **37**, 179 (1981).
[6]T. Yamabe, T. Matsui, K. Akagi, K. Ohzeki, and H. Shirakawa, Mol. Cryst. Liq. Cryst. **83**, 125 (1982).
[7]B. Kirtman, W. B. Nilsson, and W. E. Palke, Solid State Commun. **46**, 791 (1983).
[8]S. Suhai, Phys. Rev. B **27**, 3506 (1983).
[9]S. Suhai, Chem. Phys. Lett. **96**, 619 (1983).
[10]H. Teramae, T. Yamabe, and A. Imamura, J. Chem. Phys. **81**, 3564 (1984).
[11]H. O. Villar and M. Dupuis, Chem. Phys. Lett. **142**, 59 (1987).
[12]H. O. Villar, M. Dupuis, J. D. Watts, G. J. B. Hurst, and E. Clementi, J. Chem. Phys. **88**, 1003 (1988).
[13]J. L. Brédas and J. M. Toussaint, J. Chem. Phys. **92**, 2624 (1990).
[14]G. König and G. Stollhoff, Phys. Rev. Lett. **65**, 1239 (1990).
[15]J. W. Mintmire and C. T. White, Phys. Rev. Lett. **50**, 101 (1983).
[16]J. W. Mintmire and C. T. White, Phys. Rev. B **28**, 3283 (1983).
[17]M. Springborg, Phys. Rev. B **33**, 8475 (1986).
[18]M. Springborg, Phys. Scr. **T13**, 306 (1986).
[19]J. Ashkenazi, W. E. Pickett, B. M. Klein, H. Krakauer, and C. S. Wang, Synth. Met. **21**, 301 (1987).
[20]J. W. Mintmire and C. T. White, Phys. Rev. B **35**, 4180 (1987).
[21]J. W. Mintmire and C. T. White, Int. J. Quantum Chem. Symp. **21**, 131 (1987).
[22]J. Ashkenazi, W. E. Pickett, H. Krakauer, C. S. Wang, B. M. Klein, and S. R. Chubb, Phys. Rev. Lett. **62**, 2016 (1989); **63**, 1539(E) (1989).
[23]P. Vogl and D. K. Campbell, Phys. Rev. Lett. **62**, 2012 (1989).
[24]P. Vogl, D. K. Campbell, and O. F. Sankey, Synth. Met. **28**, D513 (1989).
[25]P. Vogl and D. K. Campbell, Phys. Rev. B **41**, 12 797 (1990).
[26]L. Ye, A. J. Freeman, D. E. Ellis, and B. Delley, Phys. Rev. B **40**, 6277 (1989).
[27]J. W. Mintmire and C. T. White, Phys. Rev. Lett. **63**, 2532 (1989).
[28]J. Ashkenazi, W. E. Pickett, H. Krakauer, C. S. Wang, B. M. Klein, and S. R. Chubb, Phys. Rev. Lett. **63**, 2533 (1989).
[29]R. H. Baughman, S. L. Hsu, G. P. Pez, and A. J. Signorelli, J. Chem. Phys. **68**, 5405 (1978).
[30]C. S. Yannoni and T. C. Clarke, Phys. Rev. Lett. **51**, 1191

(1983).
[31]M. Springborg and O. K. Andersen, J. Chem. Phys. **87**, 7125 (1987).
[32]M. Springborg, J. Chim. Phys. (Paris) **86**, 715 (1989).
[33]M. Springborg, Physica B **172**, 225 (1991).
[34]W. P. Su, J. R. Schrieffer, and A. J. Heeger, Phys. Rev. Lett. **42**, 1698 (1979).
[35]W. P. Su, J. R. Schrieffer, and A. J. Heeger, Phys. Rev. B **22**, 2099 (1980); **28**, 1138(E) (1983).
[36]H. C. Longuet-Higgins and L. Salem, Proc. R. Soc. London Ser. A **251**, 172 (1959).
[37]A. J. Heeger, S. Kivelson, J. R. Schrieffer, and W.-P. Su, Rev. Mod. Phys. **60**, 781 (1988).
[38]D. Baeriswyl, D. K. Campbell, and S. Mazumdar, in *Conducting Polymers,* edited by H. Kiess (Springer, Heidelberg, in press).
[39]M. Springborg, S.-L. Drechsler, and J. Málek, Phys. Rev. B **41**, 11 954 (1990).
[40]P. Hohenberg and W. Kohn, Phys. Rev. **136**, B864 (1964).
[41]W. Kohn and L. J. Sham, Phys. Rev. **140**, A1133 (1965).
[42]R. O. Jones and O. Gunnarsson, Rev. Mod. Phys. **61**, 689 (1989).
[43]B. I. Dunlap, J. W. D. Connolly, and J. R. Sabin, J. Chem. Phys. **71**, 3396 (1979).
[44]M. Springborg, Phys. Rev. B **40**, 5774 (1989).
[45]M. Springborg, Phys. Rev. B **37**, 1218 (1988).
[46]J. von Boehm, P. Kuivalainen, and J.-L. Calais, Phys. Rev. B **35**, 8177 (1987).
[47]G. Hennico, J. Delhalle, J. M. André, and J. L. Brédas, Synth. Met. **31**, 9 (1989).
[48]C. R. Fincher, Jr., C.-E. Chen, A. J. Heeger, A. G. MacDiarmid, and J. B. Hastings, Phys. Rev. Lett. **48**, 100 (1982).
[49]R. S. Mulliken, J. Chem. Phys. **23**, 1833 (1955).
[50]T. Hughbanks and R. Hoffmann, J. A. Chem. Soc. **105**, 3528 (1983).
[51]J. W. Mintmire and C. T. White, Int. J. Quantum Chem. Symp. **17**, 609 (1983).
[52]K. Smith, *The Calculation of Atomic Collision Processes* (Wiley, New York, 1971).
[53]O. Jepsen and O. K. Andersen, Solid State Commun. **9**, 1763 (1971).
[54]U. Gelius, in *Electron Spectroscopy,* edited by D. A. Shirley (North-Holland, Amsterdam, 1972), p. 311.
[55]J. W. Mintmire, F. W. Kutzler, and C. T. White, Phys. Rev. B **36**, 3312 (1987).
[56]Results of C. R. Brundle as reported by P. M. Grant and I. P. Batra, Synth. Met. **1**, 193 (1979).
[57]C. B. Duke, A. Paton, W. R. Salaneck, H. R. Thomas, E. W. Plummer, A. J. Heeger, and A. G. MacDiarmid, Chem. Phys. Lett. **59**, 146 (1978).
[58]W. R. Salaneck, H. R. Thomas, R. W. Bigelow, C. B. Duke, E. W. Plummer, A. J. Heeger, and A. G. MacDiarmid, J. Chem. Phys. **72**, 3674 (1980).
[59]W. K. Ford, C. B. Duke, and A. Paton, J. Chem. Phys. **77**, 4564 (1982).
[60]J. Rasmusson, S. Stafström, M. Lögdlund, W. R. Salaneck, U. Karlsson, D. B. Swanson, A. G. MacDiarmid, and G. A. Arbuckle, Synth. Met. **41-43**, 1365 (1991).
[61]H. Ehrenreich and M. H. Cohen, Phys. Rev. **115**, 786 (1959).
[62]S. I. Adler, Phys. Rev. **126**, 413 (1962).
[63]J. W. Mintmire and C. T. White, Phys. Rev. B **27**, 1447 (1983).
[64]J. Fink, Adv. Electron. Electron Phys. **75**, 121 (1989).
[65]J. Fink and G. Leising, Phys. Rev. B **34**, 5320 (1986).
[66]H. Fritzsche, N. Nücker, B. Scheerer, J. Fink, and G. Leising, Synth. Met. **28**, D237 (1989).
[67]W. Weyrich, Habilitationsschrift, Technische Hochschule Darmstadt, 1978 (unpublished).
[68]J.-L. Calais, Coll. Czech. Chem. Commun. **53**, 1890 (1988).
[69]L. Lam and P. M. Platzman, Phys. Rev. B **9**, 5122 (1974).
[70]M. Y. Chou, P. K. Lam, and M. L. Cohen, Phys. Rev. B **28**, 1696 (1983).
[71]D. A. Cardwell and M. J. Cooper, J. Phys. Condens. Matt. **1**, 9357 (1989).
[72]S. Rabii, J. Chomilier, and G. Loupias, Phys. Rev. B **40**, 10 105 (1989).
[73]S. Wakoh and M. Matsumoto, J. Phys. Condens. Matter **2**, 797 (1990).
[74]P. Pattison and B. Williams, Solid State Commun. **20**, 585 (1976).
[75]P. Pattison, W. Weyrich, and B. Williams, Solid State Commun. **21**, 967 (1977).
[76]A. Rozendaal, Ph.D. thesis, Vrije Universitet Amsterdam, 1985.
[77]T. Yamabe, K. Tanaka, H. Terama-e, K. Fukui, A. Imamura, H. Shirakawa, and S. Ikeda, J. Phys. C **12**, L257 (1979).
[78]M. Kertész, J. Koller, and A. Ažman, J. Chem. Soc. Chem. Commun. **1978**, 575 (1978).
[79]S. Suhai, J. Chem. Phys. **73**, 3843 (1980).
[80]M. Springborg, Synth. Met. **28**, D527 (1989).
[81]M. Springborg, H. Kiess, and P. Hedegård, Synth. Met. **31**, 281 (1989).
[82]H. Takayama, Y. R. Lin-Liu, and K. Maki, Phys. Rev. B **21**, 2388 (1980).
[83]D. Baeriswyl, D. K. Campbell, and S. Mazumdar, Phys. Rev. Lett. **56**, 1509 (1986).
[84]U. Sum, K. Fesser, and H. Büttner, J. Phys. C **20**, L71 (1987).
[85]F. W. Kutzler, C. T. White, and J. W. Mintmire, Int. J. Quant. Chem. **29**, 793 (1986).
[86]L. Ye, A. J. Freeman, D. E. Ellis, and B. Delley, Phys. Rev. B **40**, 6285 (1989).
[87]H. O. Villar, M. Dupuis, and E. Clementi, Phys. Rev. B **37**, 2520 (1988).
[88]M. Tanaka, A. Watanabe, and J. Tanaka, Bull. Chem. Soc. Jpn. **53**, 645 (1980).
[89]M. Tanaka, A. Watanabe, and J. Tanaka, Bull. Chem. Soc. Jpn. **53**, 3430 (1980).
[90]A. Feldblum, J. H. Kaufman, S. Etemad, A. J. Heeger, T.-C. Chung, and A. G. MacDiarmid, Phys. Rev. B **26**, 815 (1982).
[91]T.-C. Chung, F. Moraes, J. D. Flood, and A. J. Heeger, Phys. Rev. B **29**, 2341 (1984).
[92]Z. Vardeny, J. Orenstein, and G. L. Baker, Phys. Rev. Lett. **50**, 2032 (1983).
[93]Z. Vardeny, J. Orenstein, and G. L. Baker, J. Phys. (Paris) Colloq. **44**, C3-325 (1983).
[94]R. Fu, Z. Shuai, J. Liu, X. Sun, and J. C. Hicks, Phys. Rev. B **38**, 6298 (1988).
[95]Y. R. Lin-Liu and K. Maki, Phys. Rev. B **22**, 5754 (1980).
[96]S. A. Brazovskiĭ and N. N. Kirova, Pis'ma Zh. Eksp. Teor. Fiz. **33**, 6 (1981) [JETP Lett. **33**, 4 (1981)].
[97]D. K. Campbell and A. R. Bishop, Phys. Rev. B **24**, 4859 (1981).
[98]J. L. Brédas, R. R. Chance, and R. Silbey, Mol. Cryst. Liq. Cryst. **77**, 319 (1981).